

GEOCHEMICAL SIGNATURES FOR  
REDEPOSITIONAL ENVIRONMENTS BENEATH OXYGEN  
MINIMUM ZONES: THE BENGUELA UPWELLING  
SYSTEM OFFSHORE NAMIBIA

By

JESSICA COFRANCESCO

Bachelor of Science in Geology

California State University

Los Angeles, CA

2014

Submitted to the faculty of the  
Graduate College of  
Oklahoma State University  
in partial fulfillment of  
the requirements for  
the Degree of  
MASTER OF SCIENCE  
December, 2016

GEOCHEMICAL SIGNATURES FOR  
REDEPOSITIONAL ENVIRONMENTS BENEATH OXYGEN  
MINIMUM ZONES: THE BENGUELA UPWELLING  
SYSTEM OFFSHORE NAMIBIA

Thesis Approved:

Dr. Natascha Riedinger

---

Thesis Adviser

Dr. Eliot Atekwana

---

Dr. Mary Hileman

---

## ACKNOWLEDGEMENTS

I sincerely thank my adviser, Dr. Natascha Riedinger, for supporting me through this research. I truly appreciate all of her patience, guidance, and understanding. I thank the Boone Pickens School of Geology, the BPSofG Alumni Association, and Oklahoma State University for partial funding of this project. I also thank Dr. Jeremy Owens of Florida State University for helping with my trace metal analysis, as well as for the valuable input that he gave to me. Thank you Dr. T. Wu for advice and help in the lab. Thank you Dr. Eliot Atekwana and Dr. Mary Hileman for being on my committee and for all of your help and advice. This project would not have been the same without the Regional Graduate Network in Oceanography (RGNO) program, Dr. Kurt Hanselman and all of the international scientists, and the captain and crew of the RV MIRABILIS from the May 2015 cruise. Finally, this work would not have been possible without all of the support from my family, my husband John, and the other graduate students at Boone Pickens School of Geology, Oklahoma State University. I appreciate all of the love, help, and support that you have given to me during this exciting and challenging journey.

Name: JESSICA COFRANCESCO

Date of Degree: DECEMBER, 2016

Title of Study: GEOCHEMICAL SIGNATURES FOR REDEPOSITIONAL ENVIRONMENTS BENEATH OXYGEN MINIMUM ZONES: THE BENGUELA UPWELLING SYSTEM OFFSHORE NAMIBIA

Major Field: GEOLOGY

Abstract: Due to changes in redox environment that occur during the deposition of marine sediments, trace metal paleo-proxies have become powerful tools for reconstructing paleo-depositional environments. While there are numerous proxies for understanding endmember redox conditions, there is still a significant gap in our understanding in regards to constraining specific signals for oxygen minimum zones (OMZ) and adjacent organic-rich settings found in ancient rocks. In this study, we explore the application of geochemical and sedimentological proxies in a modern organic-rich marine OMZ system – the Benguela upwelling system off the coast of Namibia. In this upwelling system, the lateral transport of the shelf mudbelt organic-rich sediments deposited under anoxic (sulfidic) bottom waters are being redeposited under an oxygen-rich water column at the upper slope, resulting in a secondary transported organic carbon depocenter. To assess the geochemical inventory of these two different areas of organic carbon accumulation, sediment cores were collected at the shelf mudbelt and slope depocenter, using the R/V MIRABILIS. Major elements and trace metal concentrations were determined for the aqueous phase and the solid phase samples. The solid phase was also analyzed for iron speciation and grain-size distribution. The results show significant enrichments above the lithogenic background for redox sensitive trace metals such as Mo and V, and for Ni - a bioproductivity indicator. The trace metal concentrations have highest enrichments in the sediments below the anoxic bottom waters; except for Ni, which shows a higher enrichment in the bioturbated and oxygenated slope sediments compared to the oxygen-depleted, finely laminated shelf sediments of the organic-rich shelf mudbelt.

The positive correlation between nickel and total organic carbon that is observed in the sediments of upwelling zones is not maintained after lateral redeposition of the organic-rich sediments from shelf to slope in this system. The observed variations in trace metal enrichments in conjunction with high organic carbon concentrations at each site could provide a useful tool for identifying environments of organic carbon redeposition and ancient upwelling OMZs recorded in ancient rocks.

## TABLE OF CONTENTS

Chapter	Page
1. INTRODUCTION .....	1
2. METHODS .....	6
2.1 STUDY SITE .....	6
2.2 SAMPLING.....	9
2.3 SOLID PHASE ANALYSIS .....	9
2.4 AQUEOUS PHASE ANALYSIS .....	12
3. RESULTS .....	14
3.1 SOLID PHASE.....	14
3.2 AQUEOUS PHASE.....	22
4. DISCUSSION .....	25
4.1 SYSTEM REDOX ENVIRONMENTS.....	25
4.2 NI/TOC RATIOS IN UPWELLING ZONES AND REDEPOSITION .....	29
5. SUMMARY AND CONCLUSION .....	33
REFERENCES.....	36
SUPPLEMENTARY DATA .....	41
VITA.....	46

## LIST OF TABLES

Table	Page
1 Sample site information .....	9
S1 Results from sequential iron extractions.....	41
S2 Solid phase TOC, CaCO <sub>3</sub> , Al, Mn, Fe, Fe <sub>(HR)</sub> , V, Mo, and Ni.....	42
S3 Aqueous phase Fe, Mo, and V .....	43
S4 Particle size distribution.....	45

## LIST OF FIGURES

Figure	Page
1 Bathymetric map of study area offshore Namibia .....	7
2 Map of RV MIRABILIS sampling sites .....	8
3 Cartoon diagram of the Benguela Upwelling System.....	15
4 Plots of solid phase iron phases vs. core depth .....	16
5 Solid phase analysis of carbon and major elements plotted against core depth.....	18
6 Plots of solid phase V, Mo, Ni, V/Al, Mo/Al, and Ni/Al against core depth .....	19
7 Enrichment factors (EF) for V, Ni, and Mo.....	21
8 Plots of bottom and pore water Fe, Mo, and V against core depth.....	23
9 V/Mo relationship vs. core depth.....	28
10 Ni/TOC for shelf core 25020 .....	29
11 Ni/TOC for slope core Geo_Che5 .....	30
12 Core 25020 and Geo_Che5 data superimposed on Fig. from Böning et al. (2015)..	31
S1 Lithology columns with grain size distribution .....	45

## CHAPTER ONE

### INTRODUCTION

Ocean upwelling zones play a vital role in the preservation of organic carbon in sediments (Muller and Suess, 1979; Pedersen and Calvert, 1990). There are four major Eastern Boundary Upwelling Zones in today's ocean: The California Current upwelling zone, the Canary Current (Northwest Africa) upwelling zone, the Humboldt Current (offshore Peru) upwelling zone, and the Benguela Upwelling System (Philander and Yoon, 1982; Shannon and Nelson, 1996; Berger and Wefer, 2002). The four Eastern Boundary Upwelling Zones are responsible for 50% of the total primary productivity of the ocean (Skogen, 2004). In upwelling zones the wind drives the surface waters away from the shoreline through a process called Ekman Transport, and cold, nutrient rich deep water flows upward to replace it. The process of upwelling is important because the cold upwelled water brings the nutrients that sustain phytoplankton, the base of the oceanic food chain. The Benguela Upwelling System (BUS) offshore Namibia, in southwest Africa, is the most productive upwelling zone in the ocean (Shannon and Nelson, 1996). Within the BUS, the Luderitz upwelling cell at 25.5°S is the strongest upwelling cell in the entire ocean (Lutjeharms and Meeuwis, 1987).

High productivity, high sedimentation rates, and low oxygen concentrations in distinct layers of the water column are characteristics of upwelling zones that facilitate the accumulation of high amounts of organic carbon (OC) in sediments (Calvert and Pedersen, 1992). The amount of organic matter and the associated redox-sensitive trace metals that are preserved in the sediment record can provide information about the environment at the time of sediment deposition and, thus, can be used for paleo-depositional reconstruction of organic carbon-rich, fine-grained rocks, or black shales (Lipinski et al., 2003; Cruse and Lyons, 2004; Brumsack, 2006). The organic



carbon depocenter on the continental slope in the Benguela upwelling is considered a modern analogue of many Mesozoic marine black shale deposits (Calvert and Pedersen, 1992).

Variations in the enrichment or depletion of many metals (e.g. iron (Fe), molybdenum (Mo), and vanadium (V)) in the sedimentary record reflect the oxygen concentration or sulfur species present in the bottom water during deposition (Böning et al., 2015; Tribovallard et al., 2006). Iron is a bioessential element for all life on the planet. The iron oxyhydr(oxide) phase is the most reactive element in aquatic environments (e.g., Viollier et al., 2000) so the amount and availability of this iron phase affects the distribution of trace elements in marine sediments (Alvarez-Iglesias and Rubio, 2009). The iron oxyhydr(oxide) phase is the prominent metal oxide reduction process coupled to organic matter oxidation, a transport mechanism for Mo, and is a key component in pyrite formation (Raiswell and Canfield, 2012). Pyrite ( $\text{FeS}_2$ ) is formed from iron oxide phases in the presence of dissolved sulfides and this can occur in both the sediment and in the water column (Berner, 1970; Raiswell and Canfield, 1998). Because of the chemical reactions that form pyrite, the quantity and speciation of iron in sediments and sedimentary rocks can provide important information about the redox conditions of the local depositional environment (Raiswell and Canfield, 2012).

Trace metals such as Mo, nickel (Ni), and V accumulate in sediments in upwelling zones and have two major enrichment pathways: 1) seawater sourced metals related to the redox conditions in the water column and bottom water which relates to the size and position of the oxygen minimum zone (OMZ), and 2) biologically sourced metals contained in the organic matter related to the high productivity (Tribovillard et al., 2006). The use of Mo as a paleo-redox proxy is based on its distinctive geochemical behavior in both oxic and sulfidic environments (e.g., Alego and Lyons, 2006). In oxygenated waters, Mo speciation is dominated by the Mo(VI) species in the form of the molybdate anion ( $\text{MoO}_4^{2-}$ ), which is unreactive such that Mo is the most abundant transition metal in seawater (Brumsack, 1989; Emerson and Huested, 1991). In oxic waters, Mo

from seawater adsorbs onto Fe and Mn-(oxyhydr)oxides at the sediment/water interface (SWI) (Shimmield and Price, 1986; Crusius et al., 1996). If reducing conditions occur, the reduction of the Fe and Mn-(oxyhydr)oxides releases the scavenged Mo to the sediment pore water, creating a porewater concentration gradient and a downward diffusive flux (Crusius et al., 1996). An additional reduction step from Mo(VI) in molybdate ( $\text{MoO}_4^{2-}$ ) to the intermediate phase Mo(V) occurs when the oxygen atoms are replaced with sulfur atoms in the presence of  $\text{HS}^-$  and form oxythiomolybdates ( $\text{MoO}_x\text{S}_{4-x}$ ) ( $x=1-4$ ). This is the geochemical “switch” that must occur in order for Mo to be fixed to the sediment as Mo(IV) in molybdenite ( $\text{MoS}_2$ ) (Helz et al., 1996). The switch is achieved by the presence of over 100  $\mu\text{M}$   $\text{HS}^-$ , which causes Mo to be scavenged to the sediments through co-precipitation with iron sulfides and complexation with sulfur-rich humic materials (Brumsack, 1989; Emerson and Huested, 1991; Crusius et al., 1996). Consequently, Mo concentrations have been used in a number of studies to distinguish between environments with differing redox conditions in the bottom water (Helz et al., 1996; Nameroff et al., 2002; Lipinski et al., 2003; Cruse and Lyons, 2004; Borchers et al., 2005; Algeo and Lyons, 2006; Scott and Lyons, 2012).

Vanadium (V) is a redox-sensitive trace element that is enriched in the sediments of both suboxic and anoxic environments and again during diagenesis, which results in V enrichments in black shales with high organic matter content (Tribovillard et al., 2006). In oxygenated seawater, V exists as V(V), in the form of the vanadate oxyanion ( $\text{H}_2\text{VO}_4^-$ ) or ( $\text{HVO}_4^{2-}$ ), and can easily adsorb onto Fe and Mn-(oxyhydr)oxides (Emerson and Huested, 1991; Tribovillard et al., 2006). Under mildly reducing conditions, V(V) is reduced to V(IV) and forms vanadyl ions ( $\text{VO}^{2+}$ ), related hydroxyl species (e.g.  $\text{VO}(\text{OH})_3^-$ ), and insoluble hydroxides ( $\text{VO}(\text{OH})_2$ ) (Algeo and Maynard, 2004; Tribovillard et al., 2006). The insoluble hydroxides precipitate when facilitated by the presence of humic and fulvic acids (Wilson and Weber, 1979). The V(IV) species can be removed from the pore water and adsorbed to the sediment surface by the formation of

organometallic ligands (Emerson and Husted, 1991). In the presence of free  $\text{HS}^-$  under stronger reducing conditions, V(IV) is further reduced to V(III) and precipitated out to the sediments as a solid oxide ( $\text{V}_2\text{O}_3$ ) or hydroxide ( $\text{V}(\text{OH}_3)$ ) phase (Emerson and Husted, 1991), or incorporated into the central atom position to replace magnesium (Mg) in porphyrins, the diagenetic products of chlorophyll (Callot et al., 1990). Because of the two-step reduction process necessary for V fixation in the sediment, V concentrations combined with Mo concentrations are used to elucidate information regarding very subtle changes in redox environments (Algeo and Maynard, 2004).

Copper (Cu), nickel (Ni), and zinc (Zn) are the trace metals that are associated with biocycling processes and bioproductivity (Borchers et al., 2005). These metals are all micronutrients (Martin and Knauer, 1973) and are delivered to the sediments directly with the sinking biodebris (Brongersma Sanders, 1980; Böning et al., 2015). If the redox environment of the sediments is reducing enough to contain free sulfide, then Cu and Zn will quickly precipitate out of solution to form sulfide minerals (Jacobs and Emerson, 1985) while Ni does not (Morse and Luther, 1999). This makes Ni a better proxy for productivity because it is not redox sensitive. Nickel is an element that is associated with the opaline frustules of diatoms (Twining et al., 2012). A unique characteristic of Ni in reducing sediments is that Ni does not readily form insoluble compounds with sulfides like Cu and Zn, but is retained with the OM that it was initially deposited with (Böning et al., 2015). Like V, Ni is also a central atom in porphyrins and becomes enriched during diagenesis. For these reasons Ni is a good indicator of a high OM flux, even if the original OM has been remineralized by bacterial oxidation or reoxygenation (Tribovillard et al., 2006; Böning et al 2015).

By using the pore water concentrations of Mo and V, in concert with the solid phase concentrations of the highly reactive iron oxy(hydr)oxide phase ( $\text{Fe}_{\text{HR}}$ ), V, and Mo a more complete picture of the redox environment in the overlying water column can be established. Then, through the combination of sedimentological observations from recent organic-rich

sediments and trace metal geochemical measurements of Ni, a metal associated with sinking OM and productivity, a much more complete view of the depositional environment can be obtained. The results from this study will provide a useful tool for identifying environments of organic carbon redeposition and upwelling related oxygen minimum zones recorded in ancient rocks.

## CHAPTER TWO

### METHODS

#### 2.1 STUDY SITE

Sediments were collected from the Benguela upwelling system offshore Namibia in southwestern Africa (Fig. 1). The BUS is one of four major eastern boundary upwelling zones and it is the most productive coastal upwelling region of the ocean (Shannon and Nelson, 1996). The phytoplankton that live in the coastal waters covering the Namibian shelf are dominated by diatoms, dinoflagellates, and radiolarians while the waters above the shelf edge upwelling area are rich with coccolithophores and foraminifera (Pitcher et al., 1991; Giraudeau et al., 1993; Schmidt and Eggert, 2012). The perennial upwelling that occurs in the BUS supports the high primary production (estimated to be 0.37 Gt/yr.) which, in turn, creates extreme water column oxygen depletion and periodic sulfidic bottom water from the *in-situ* degradation of this sinking biodegradable material (Carr, 2002). The result of this type of process is a very wide OMZ which stretches from the shelf far across to the upper continental margin (Summerhayes et al., 1995; Mollenhauer et al., 2007). Large areas of organic carbon preservation occur in these sediments (Calvert and Price, 1981; Summerhayes et al., 1995; Mollenhauer et al., 2002). On the shelf there is a narrow mudbelt of organic carbon-rich diatomaceous ooze (Summerhayes et al., 1995) and a prominent depocenter of organic carbon also exists between 24.5° and 26° S on the upper continental slope in water depths of 400 m-1500 m (Fig. 1) (Inthorn et al., 2006a; 2006b). Inthorn et al. (2006b) stated that the shelf mudbelt was the source of the organic matter presently accumulating on the slope depocenter, and that lateral (offshore) sediment transport in nepheloid layers was the mechanism transporting the sediments from the shelf to the slope.

The surface waters off Namibia (Fig. 2) are influenced by the Benguela Current System which consists of two branches, the Benguela Oceanic Current and the Benguela Coastal Current (Summerhayes et al., 1995). Southeasterly trade winds induce the upwelling of cold nutrient-rich South Atlantic Central Waters (SACW) close to the shore, generally from water depths of 50-200 m (Shannon, 1985). At 25.5° S, the perennial Lüderitz cell is the strongest upwelling cell of the BUS (Lutjeharms and Meeuwis, 1987).

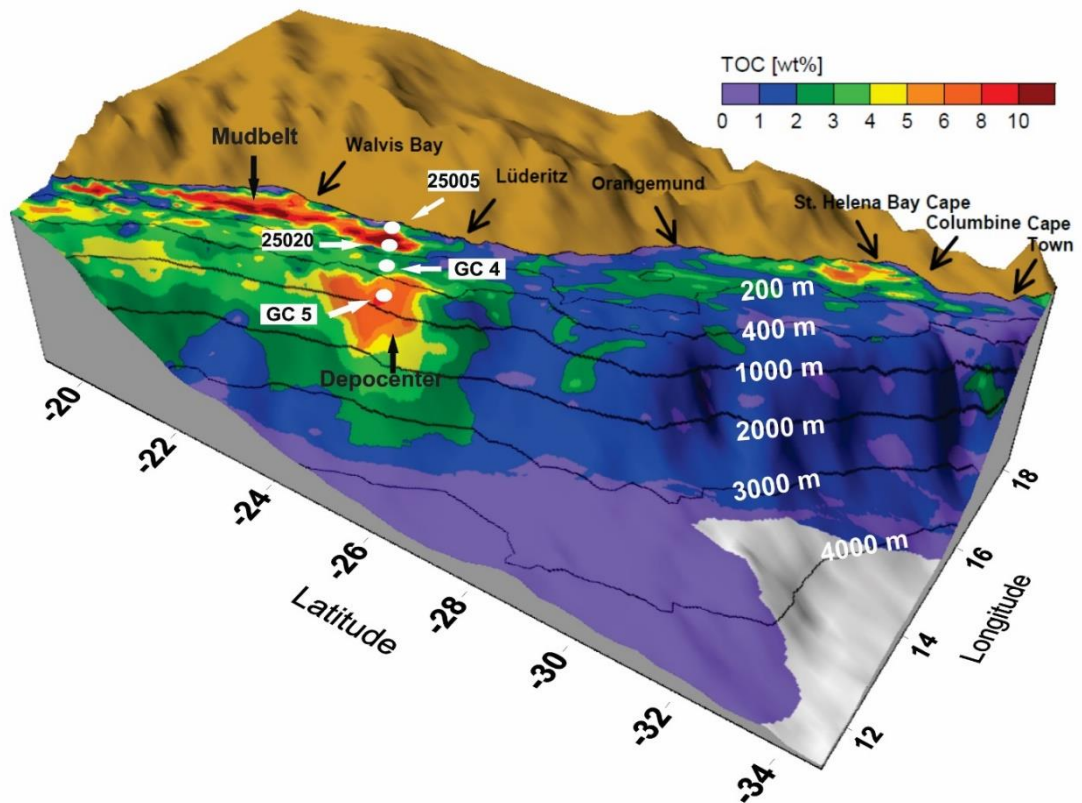


**Figure 1:** Bathymetric map of the study area offshore Namibia showing the areas of organic carbon preservation (warmer colors) in the sediments (modified after Inthorn et al., 2006). The samples for this study, shown as white filled circles, were taken from the shelf mudbelt (core 25005 from the near-shore edge of the mudbelt and core 25020 from the center of the mudbelt) and the slope depocenter (core GC5 is short for Geo\_Che5). Core Geo\_Che4 (GC4) was taken from the outer shelf break, which is an area in between the two prominent centers of organic carbon preservation.

Eddies and filaments of nutrient-rich water carry some of the high-productivity water offshore and over much of the slope region (Robinson et al., 2002). Below the water depth of 100 m, the South Atlantic Central Water (SACW) provides the poleward undercurrent that drives the deeper waters to the southeast (Robinson et al., 2002).

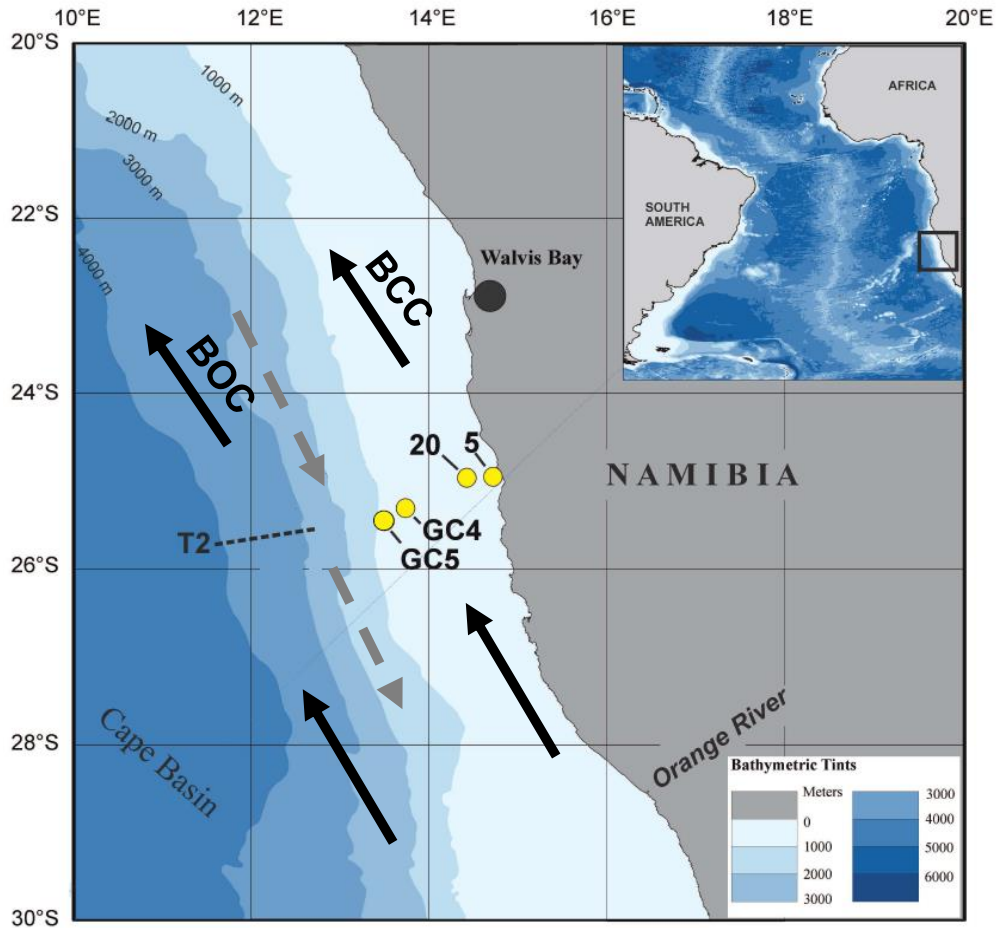


**Figure 2:** Map showing the location for RV MIRABILIS sampling sites in yellow filled circles. The short dashed line marks the transect T2 along the 25.5°S line. Cores 25005, 25020 are displayed as 5 and 20, respectively, and Geo\_Che4 is GC4 and Geo\_Che5 is GC5. Surface currents of the Benguela system, the Benguela Coastal Current (BCC) and the Benguela Oceanic Current (BOC) are indicated by black arrows, and the undercurrent that flows over the outer shelf towards the south is indicated by gray dashed arrows. Figure modified from (Riedinger et al., 2006).

There is also the occurrence of shelf edge upwelling of the cold, nutrient rich Antarctic Intermediate Water (AAIW), which is separate from the inshore frontal current bounding the coastal upwelling centers over the inner shelf (Summerhayes et al., 1995). This second upwelling area provides the nutrients for the additional productivity occurring over the upper slope (Summerhayes et al., 1995).

## 2.2 SAMPLING

Sediment cores were collected via the RV MIRABILIS as part of the May 2015 Regional Graduate Network in Oceanography (RGNO) program in Namibia. Surface sediment was retrieved using a multicorer (MUC) device. Core 25005 was obtained from the shelf at a water depth of 49 m; core 25020 was obtained from the shelf at a water depth of 116 m; core Geo\_Che4 was obtained from the outer shelf break at a water depth of 302 m; and core Geo\_Che5 was obtained from the slope at a water depth of 795 m (Table 1). The cores were immediately sliced onboard the ship into 1-2 cm intervals for the length of the entire core (24-28 cm). The sediments were transferred into 50 mL centrifuge tubes and the head space was purged with N<sub>2</sub> gas before sealing in order to prevent oxygen exposure to the sediment. The sediment samples were stored frozen at -20°C in order to slow down microbial activity.

**Table 1.** Station, position, water depth, bottom water oxygen concentration, and relativity to oxygen minimum zone (OMZ) for sampling sites.

<b>Station</b>	<b>Latitude</b>	<b>Longitude</b>	<b>Water depth (m)</b>	<b>Bottom water oxygen (mL/L)</b>	<b>Site position relative to OMZ</b>
<b>25005</b>	25°00.000'S	14°44.400'E	49	0.05	In the OMZ
<b>25020</b>	25°00.000'S	14°28.200'E	116	0.05	In the OMZ
<b>Geo_Che4</b>	25°20.660'S	13°46.480'E	302	1.11	In the OMZ
<b>Geo_Che5</b>	25°30.000'S	13°27.000'E	795	3.36	Below the OMZ

## 2.3 SOLID PHASE ANALYSIS



### 2.3.1 IRON PHASES

A sequential iron extraction (modified after Poulton and Canfield, 2005; Raiswell et al., 2010) was performed in an anaerobic chamber using 0.3 g of frozen sample in 10 mL of each extraction solution. The amount of iron present as reactive iron oxides ( $\text{Fe}_{\text{HR}}$ ) was calculated as the sum of the concentrations obtained from the three iron extraction steps that were used: 1) sodium acetate for the carbonate associated phases (siderite and ankerite/ferroan dolomite) (Tessier et al., 1979), 2) sodium dithionate for the crystalline oxides (goethite and hematite), and 3) ammonium oxalate for the iron associated with magnetite (Raiswell et al., 1994). The sodium acetate solution is a 1M sodium acetate ( $\text{C}_2\text{H}_3\text{NaO}_2$ ) solution buffered with acetic acid ( $\text{CH}_3\text{COOH}$ ) to pH of 4.5. The 0.3 g of sediment with the 10 mL of acetate solution are mixed in a mixer for 24 hours, placed in a centrifuge for 5 minutes each at 5500 rpm, and 4 mL is decanted for analysis. The sodium dithionate solution is a 50  $\text{gL}^{-1}$  sodium dithionite ( $\text{Na}_2\text{S}_2\text{O}_4$ ) solution buffered with 0.35 M acetic acid and 0.2 M sodium citrate ( $\text{Na}_3\text{C}_6\text{H}_5\text{O}_7 \cdot \text{H}_2\text{O}$ ) to a pH of 4.8. The same tube with the sediment from the first step with 10 mL of the dithionite solution is then mixed in a mixer for 2 hours, placed in a centrifuge for 5 minutes each at 5500 rpm, and 4 mL is decanted for analysis. The ammonium oxalate solution is a 0.2 M ammonium oxalate ( $\text{C}_2\text{H}_8\text{N}_2\text{O}_4 \cdot \text{H}_2\text{O}$ ), 0.17 M oxalic acid ( $\text{H}_2\text{C}_2\text{O}_4 \cdot 2\text{H}_2\text{O}$ ) solution buffered with ammonium hydroxide to pH 3.2. The same tube with the sediment from the first two steps with 10 mL of the ammonium oxalate solution is then mixed in the mixer for 6 hours, placed in a centrifuge for 5 minutes each at 5500 rpm, and 4 mL is decanted for analysis. The ferrozine method (Stookey, 1970) was used to determine the iron concentrations for each extraction step with a spectrophotometer. The reproducibility of each extraction step was within 5%, which was determined through the analysis of duplicate samples. A 3 g split of each sample was also dried in an oven and re-weighed to determine the water weight. All concentrations are reported in dry weight basis.

### 2.3.2 ORGANIC AND INORGANIC CARBON PHASES

The total organic carbon (TOC) concentration of the sediments were measured after pre-treatment with HCl to remove any inorganic carbon. An 8-15 mg split of each core interval was oven dried at 40°C for 72 h, homogenized, and weighed on an analytical scale inside a pressed silver capsule. Samples were analyzed using a Costech Elemental Analyzer (EA).

Calcium carbonate concentrations ( $\text{CaCO}_3$ ) of the solid phase samples were measured according to the methods of Krishnamurthy et al. (1997). A known amount of homogenized sample was added to a 10 mL vacutainer septum tube, and a Pyrex boat was glued to the inside of the tube. Approximately 1 mL of 100% phosphoric acid was then added to the Pyrex boat and the septum was put back into place to seal the tube. The tubes were then evacuated on the vacuum line through use of a needle assembly. After the required vacuum conditions were established, the tubes were placed in a 25° C water bath for 30 minutes, in order for both the acid and the sample to reach thermal equilibrium. While still in the bath, the tubes were then tilted to allow the acid to drain out of the boat and cover the sample. The reacting mixture was kept in the 25° C water bath for 6 hours before extraction. The reaction products, water and  $\text{CO}_2$ , were extracted from the septum tubes under vacuum. The  $\text{CO}_2$  was purified cryogenically, and yield measured manometrically by a pressure transducer. From the yield of  $\text{CO}_2$  the percentage of carbonates in the samples was calculated.

### 2.3.3 TRACE METALS

The major elements measured in the sediments were Al, Mn, and Fe, and the trace metals measured were V, Mo and Ni. A three-acid digestion using concentrated trace metal grade

hydrochloric acid, nitric acid, and hydrofluoric acid (HCl, HNO<sub>3</sub>, HF) was performed using a microwave system on 50 µg homogenized dry sample. Samples were analyzed upon 50-fold dilution (trace metal grade 2% HNO<sub>3</sub>) on a Thermo Element II Inductively Coupled Plasma-Mass Spectrometer (ICP-MS) using He in the collision cell. Sample preparation and analyses were carried out at Florida State University. A set of standard reference materials (NIST 2702, SDO1, and SCO1) were digested and analyzed with each set of samples in order to verify the precision of the instrument and, in all cases, were within the accepted analytical error for all elements measured.

The concentrations of trace metals and TOC in sediments containing variable amounts of biogenic opal and CaCO<sub>3</sub> can become diluted (Borchers et al., 2005; Tribovillard et al., 2006). In order to make the results easier to interpret enrichment factors (EF's) are used. The EF is calculated as:  $EF_X = (X/Al_{\text{sample}}) / (X/Al_{\text{avg. crust}})$  (McLennan, 2001). If an element has an EF that is greater than 1, it is enriched. Likewise, if the element has an EF that is less than 1, it is depleted.

#### 2.3.4 PARTICLE SIZE ANALYSIS

For grain size analysis, 5 g of dried and homogenized sample was pre-treated with a 10% w./v., a 20% w./v., and a 30% w./v. H<sub>2</sub>O<sub>2</sub> solution to remove organic matter (Allen and Thornley, 2004). To remove the biogenic silica from the sediments, samples were soaked for one hour in a 1M sodium hydroxide (NaOH) solution in an 85°C water bath (DeMaster, 1981). For the removal of calcium carbonate (CaCO<sub>3</sub>) samples were treated with 20% w./v. HCl (Kunze and Dixon, 1986). Prior to analysis on a Cilas 1180 particle size analyzer, samples were soaked overnight in a 5% sodium hexametaphosphate suspension solution.

## 2.4 AQUEOUS PHASE ANALYSIS

### 2.4.1 PORE WATER TRACE METALS

Depth measurements of ocean water temperature, salinity, and bottom water oxygen levels were obtained with a Conductivity Temperature Depth (CTD) instrument onboard the ship. The lowermost cast was generally within 1 meter above the seafloor. For analysis of the bottom water trace metals, samples were immediately extracted from the top of each sediment core tube with a 50 mL syringe. For analysis of sediment pore water trace metals, the pore water was extracted from each tube containing sediments via a Rhizon (Seeberg-Elverfeld et al., 2005) connected to a 30 mL syringe through an airtight and pre-drilled hole in the top of each centrifuge tube. All water samples were acidified with concentrated trace metal grade nitric acid. The 46 bottom and pore water samples were refrigerated at 4°C. Samples were analyzed for trace metals using an Inductively Coupled Plasma-Mass Spectrometer (ICP-MS; Thermo Fisher Scientific iCAP Q). All samples were diluted 50-fold prior analysis using 2% trace metal grade HNO<sub>3</sub>. A set of standard reference materials (NIST 1643f) was analyzed with each set of samples; the standard deviation for the concentration of all elements was <5%.

## CHAPTER THREE

### RESULTS

#### 3.1 SOLID PHASE

Sediments from the inner shelf mudbelt (site 25005) are green/black in color and have a strong sulfur odor. Shell fragments and fine laminations were visible below the core depth of 14 cm (Fig. S1A). Mudbelt sediments from site 25020 are also green/black in color with a strong sulfur odor. However, this core has fine laminations from the top of the core to the core bottom. Sediments consist of interbedded fine and coarse silt, and below 20 cm core depth, the grain size decreases to a fine silt that contains shell fragments (Fig. S1B). Site Geo\_Che4 is on the shelf break between the organic rich areas and the sediments are brown/black in color and have no sulfur odor or laminations. Tubes/worms were observed in the core top and the bottom half of the core contains shell fragments (Fig. S1C). The upper slope sediments from site Geo\_Che5 are green/black in color and are not laminated. Shell fragments are visible from 8 cm core depth to the core bottom (Fig. S1D).

##### 3.1.1 PARTICLE SIZE DISTRIBUTION

The results of the particle size analysis are found in the supplementary data section, in Table S4. Information from a general core description and the particle size data was used to create a lithology column figure for each core (Figure S1A-S1D). Additionally, there are summarized lithology columns plotted next to the depth distribution figures for the trace metals in both solid and aqueous phase. A general diagram of the BUS as it applies to this study was then created (Fig. 3) using the general core description in combination with the particle size analysis and water column oxygen data.

### 3.1.2 IRON PHASES

Iron phase data are shown in Table S1. Inner slope sediments (core 25005) show a clear decrease downcore in the concentration of all the iron phases except in the magnetite forming iron phase, which shows a downcore increase in concentration (Fig. 4A). Mudbelt sediments (core 25020) show an overall downcore increase in all of the highly reactive ( $Fe_{HR}$ ) iron phases (Fig. 4B).

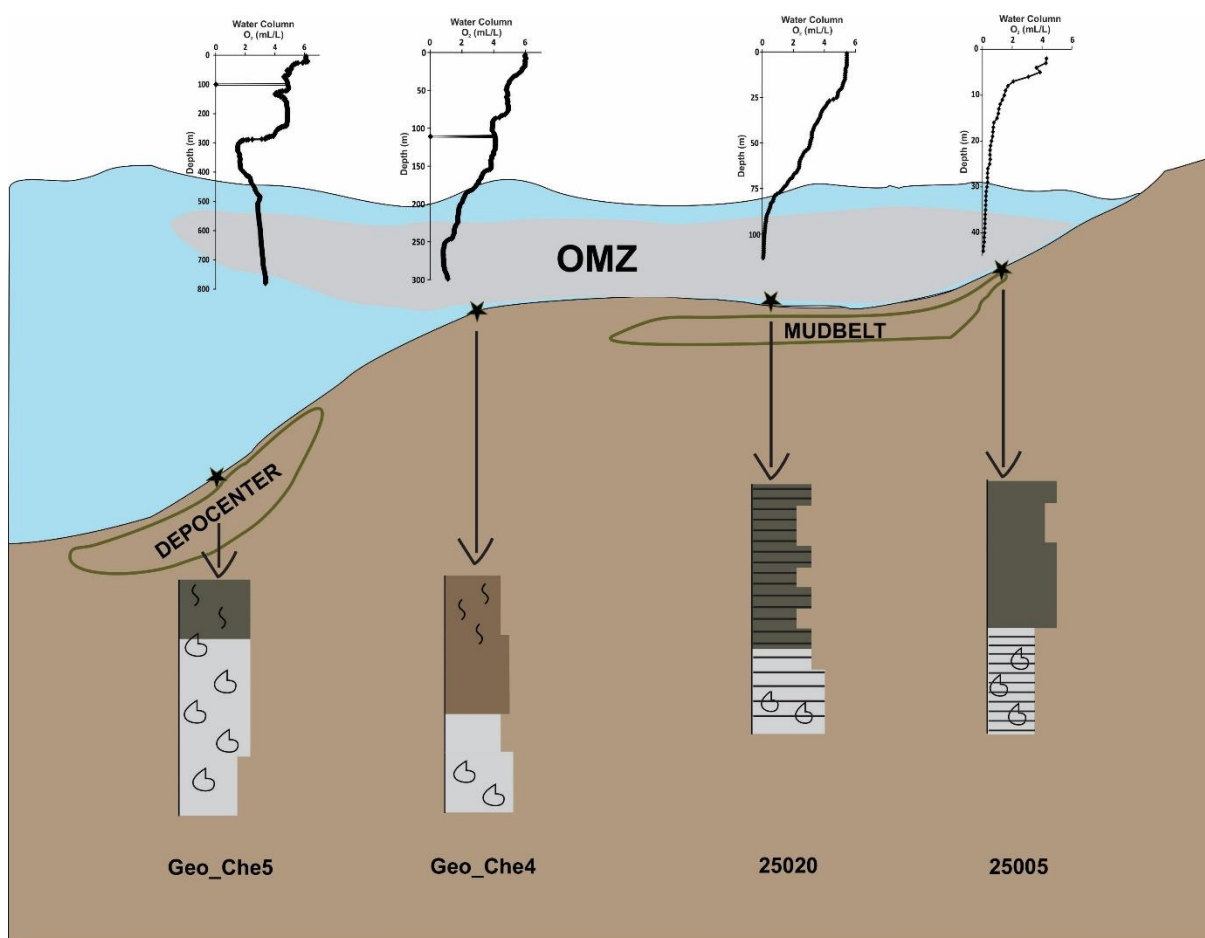


**Figure 3:** Diagram of the Benguela Upwelling System from this study (not to scale) and the core locations with respect to their positions in proximity to the oxygen minimum zone (OMZ) and the areas of organic carbon preservation. Each core location (represented by black stars) has the corresponding water column oxygen concentrations directly above it, as measured by the CTD onboard the R/V MIRABILIS, and the corresponding lithology column. The boundaries of the OMZ, in grey, were determined by the water column oxygen profiles above each core site.

In the sediments from core Geo\_Che4 there is a clear decrease in all available iron concentrations downcore for all iron phases except the magnetite forming iron phase (Fig. 4C). The slope sediments (core Geo\_Che5) show no clear downcore trends (Fig. 4D).

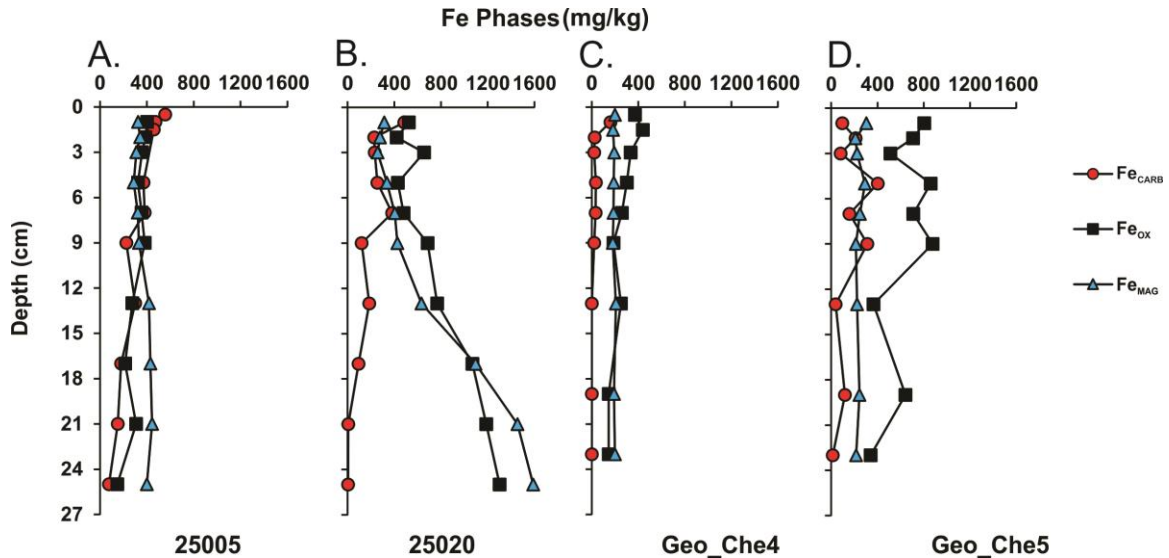


**Figure 4:** Plots of solid phase iron phases vs. core depth (above) for the 3 step iron extraction using acetate to extract carbonate related iron phases (Fe<sub>CARB</sub>; red circles), dithionate to extract crystalline oxide related iron phases (Fe<sub>OX</sub>; black squares), and ammonium oxalate to extract iron related to magnetite (Fe<sub>MAG</sub>; blue triangles) for cores (A) 25005 (B) 25020 (C) Geo\_Che4 and (D) Geo\_Che5.

### 3.1.3 ORGANIC AND INORGANIC CARBON

Inner slope sediments (core 25005) have organic carbon contents ranging from 1-4 wt.% (Fig. 5A) and calcium carbonate (CaCO<sub>3</sub>) contents ranging from 2-6 wt.%. The average organic carbon concentration of the mudbelt sediments (core 25020) is 9 wt.% with a CaCO<sub>3</sub> content ranging from 7-17 wt.% (Fig. 5B). Sediments from the shelf break (core Geo\_Che4) have an average of 3% TOC and CaCO<sub>3</sub> amounts range from 23-36 wt.% (Fig. 5D). The average organic carbon concentration on the slope (core Geo\_Che5) is 8 wt.% and the CaCO<sub>3</sub> contents range from 35-63 wt. % (Fig. 5D).

### 3.1.4 MAJOR ELEMENTS AND TRACE METALS

The contents of Al, Ba, Mn, Fe, and Fe oxides as well as the trace metals Mo, Ni, and V are

presented in Table S2. The contents of solid phase major elements and trace metals are each plotted against Al in order to normalize the data against the lithogenic background. Sediments from core 25005 have an average Al content of 3.5 wt. % for the entire length of the core (Fig. 5A). The content of Mn ranges from 400-557 mg/kg downcore to a core depth of 12 cm, after which the Mn content decreases downcore to 125 mg/kg by the core bottom. The Fe content in sediments from core 25005 average 2.5 wt.% for the entire length of the core. The mudbelt sediments (core 25020) have Al contents ranging from 0.9-3.6 wt.% with a noticeable spike at a core depth of 9 cm (Fig 5B). Manganese content averages 75 mg/kg and iron content averages 1.0 wt. % for the entire core. On the shelf break the sediments have average Al contents of 1.2 wt. % (Fig. 5C), average Mn contents of 80 mg/kg, and average Fe contents of 1.4 wt. % for the entire length of the core. Sediments in the slope core (Geo\_Che5) have average Al contents of 1.6 wt. %, average Mn contents of 70 mg/kg, and average Fe contents of 1.0 wt. % for the entire core (Fig. 5D).

The V contents of sediments from core 25005 are decreasing downcore from 130 mg/kg at the core top to 51 mg/kg at a core depth of 21 cm, followed by an increase in V to 63 mg/kg at the core bottom (Fig. 6A). Molybdenum contents are 8 mg/kg at the core bottom. There is a spike in the Mo content at a core depth of 17 cm to 12 mg/kg. The content of Ni is 33 mg/kg at 13 cm core depth, followed by an increase to 143 mg/kg from 13-21 cm core depth, and a decrease to 43 mg/kg by the core bottom. In the mudbelt sediments (core 25020) the content of V is 47 mg/kg at the core top (Fig. 6B). At a core depth of 2 cm the V content decreases to 37 mg/kg, followed by an increase with depth (37-42 mg/kg) by a core depth of 21 cm, after which the V content increases to 200 mg/kg by the core bottom. A spike in the V content to 92 mg/kg at a core depth of 9 cm is observed, corresponding to an increase in Al at this depth.



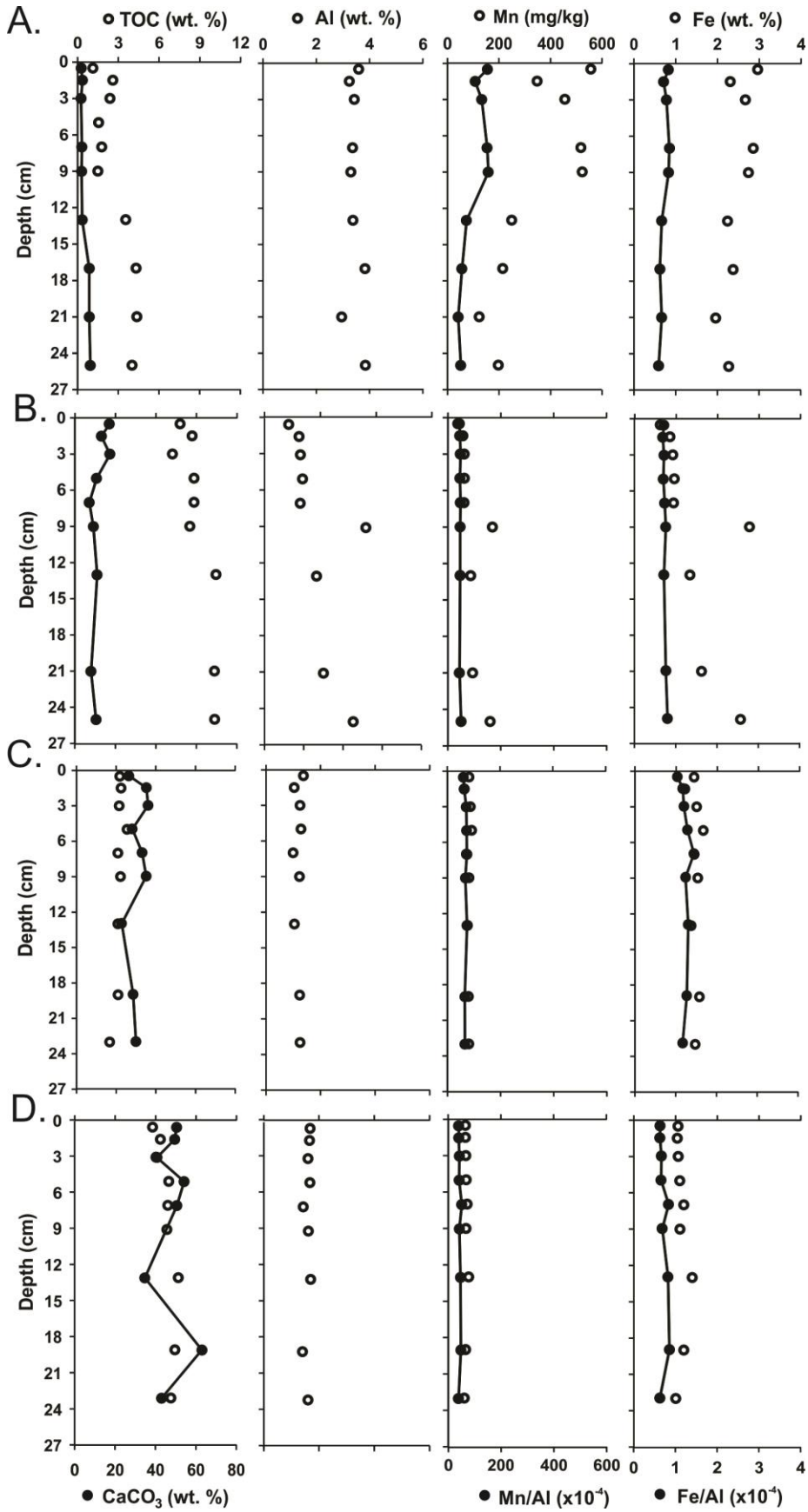


**Figure 5:** (previous page) Solid phase analysis of carbon and major elements plotted against core depth for (A) core 25005 (B) core 25020 (C) core Geo\_Che4 and (D) Geo\_Che5. Plots depict the concentrations of calcium carbonate ( $\text{CaCO}_3$ ) (closed circles with lines), total organic carbon (TOC), Al, Mn, and Fe, (open circles). The Mn and Fe contents (closed circles with lines) are also plotted against Al to normalize results for the lithogenic background.

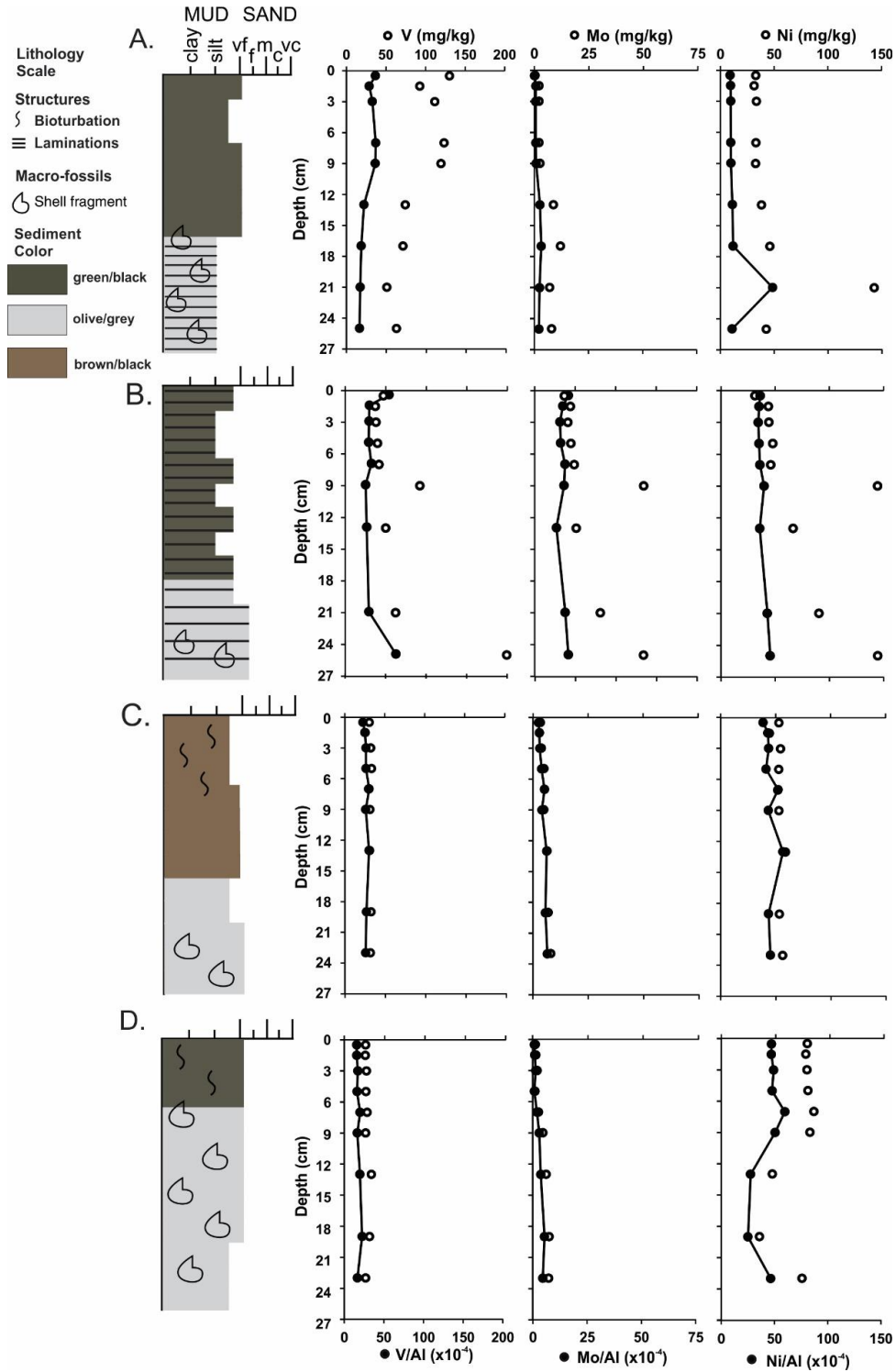


**Figure 6:** (*previous page*) Plots depicting in mg/kg solid phase V, Mo, and Ni contents (open circles), and V/Al, Mo/Al, and Ni/Al ratios (closed circles with lines) against core depth for (A) core 25005 (B) core 25020 (C) core Geo\_Che4 and (D) core Geo\_Che5.

The Ni content in core 25020 is lowest (31 mg/kg) at the core top and increases with sediment depth to 144 mg/kg by the core bottom (Fig. 6B). The Mo content is also lowest (18 mg/kg) at the core top and increases downcore (to 67 mg/kg). It is noteworthy that there is a sudden decrease (67-26 mg/kg) in the Mo content at a core depth of 13 cm, after which it increases back to 67 mg/kg by the core bottom (Fig. 6B). Sediments from core Geo\_Che4 have V contents ranging from 30-34 mg/kg for the entire length of the core, with one exception at a core depth of 2 cm in which the content of V decreases to 26 mg/kg (Fig. 6C). The Mo content is 3 mg/kg in the upper 2 cm of this core, then increases downward to 5 mg/kg by a core depth of 9 cm. From a core depth of 13 cm to the core bottom, the content of Mo ranges from 6-8 mg/kg. The content of Ni in the shelf break sediments (core Geo\_Che4) ranges from 53-55 mg/kg from the core top to a depth of 9 cm, except at a core depth of 2 cm, where the Ni content decreases to 44 mg/kg. At 13 cm core depth, the Ni content increases to 59 mg/kg, then decreases to 54 mg/kg by the core depth of 19 cm, before increasing to 57 mg/kg at the core bottom. The slope sediments (core Geo\_Che5) have V content ranging from 26-28 mg/kg for the entire length of the core (Fig. 6D). The Ni contents range from 78 to 80 mg/kg in the first 5 cm of core, followed by an increase to 85 mg/kg (at 7 cm core depth), and a decrease to 74 mg/kg by the core bottom. The Mo content is lowest at the core top (1-2 mg/kg) and increases downcore (to 9 mg/kg at 9 cm core depth) before decreasing (to 7 mg/kg) by the core bottom.

### 3.1.5 TRACE METAL ENRICHMENT FACTORS

The sediments in core 25005 are showing slight enrichments for V (average EF= 2.1), Ni (average EF=2.7), and Mo (average EF=3.4) (Fig. 7). Shelf mudbelt sediments (core 25020) are slightly enriched in V (average EF=2.7), enriched in Ni (average EF=6.9), and highly enriched in

Mo (average EF=22.9). In core Geo\_Che4, the enrichment of V (average EF=2.0) and Mo (average EF=3.5) has only decreased slightly compared to core 25020, while the enrichment of Ni (average EF=8.2) is continuing to increase. On the slope there are enrichments of V (average EF=1.3) and Mo (average EF=2.0) with Ni enrichments continuing to increase (average EF=9.1).

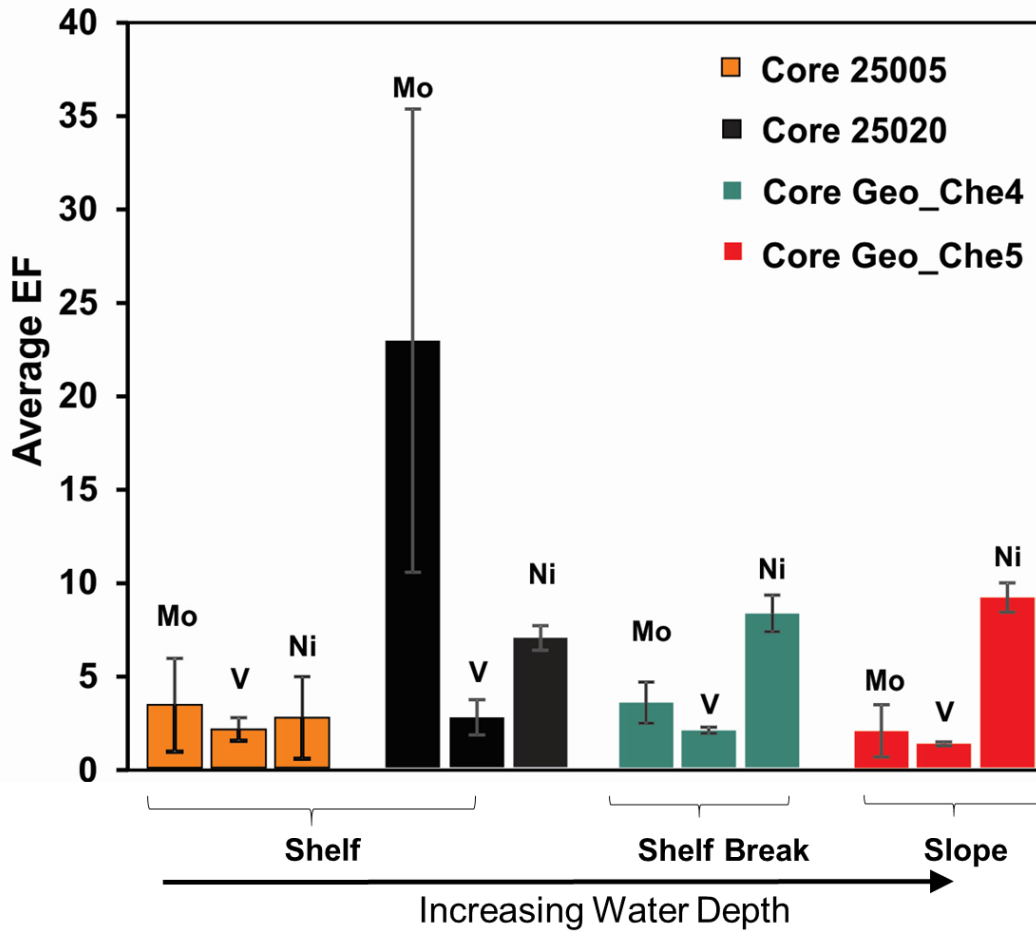


**Figure 7:** Enrichment factors (EF) for V, Ni, and Mo for core 25005 in orange, core 25020 in black, core Geo\_Che4 (GC4) in green, and core Geo\_Che5 (GC5) in red. Enrichments were normalized against Al and calculated using average upper crust values. The EF for each element represents the average for the entire core and the error bars represent the standard deviations.

### 3.2 AQUEOUS PHASE RESULTS

The CTD measured the bottom water from the lowermost cast at each site, which was within 1 m from the seafloor. The bottom water at sites 25005 and 25020 within the OMZ in water depths of 49 m and 116 m, respectively, had O<sub>2</sub> concentrations below the CTD detection limit of 0.05

mL/L. Bottom water from site Geo\_Che4 at 302 m water depth contained 1.1 mL/L O<sub>2</sub>, while bottom water from site Geo\_Che5 at 795 m water depth contained 3.4 mL/L O<sub>2</sub> (Table 1).

The pore water and bottom water trace metal data is found in Table S3. In core 25005 the concentration of pore water Fe stays below 1 µM to a core depth of 13 cm, where the concentration increases to 1.3 -1.9 µM through the remainder of the core (Fig. 8A). Dissolved Mo concentrations in core 25005 are 34 nM at the top of the core, and decrease to below the detection limit by a core depth of 7 cm (Fig. 8B). Mo concentrations increase to 186 nM by 13 cm core depth, then fluctuate downcore between 250 nM and 39 nM. Dissolved V concentrations increase from 35 nM in the bottom water to 73 nM by a core depth of 3 cm, before sharply decreasing to 4 nM by 7 cm core depth (Fig. 8B). At 9 cm core depth, the pore water V concentration begins increasing downcore to 310 nM at 13 cm core depth, before fluctuating between 45 nM and 213 nM until the core bottom. The Fe concentration for core 25020 is <1 µM in the bottom water and increases to 11 µM by a core depth of 3 cm before decreasing downcore to less than 1 µM by the core bottom (Fig. 8A). The concentration of Mo is 120 nM in the bottom water, followed by a decrease downcore to 1 nM by 13 cm core depth, and an increase at 17 cm core depth 151 nM. At the core bottom, the concentration of Mo is 107 nM. Dissolved V concentrations are 117 nM in the bottom water and decrease to 38 nM at 3 cm core depth, followed by fluctuations between 17 -65 nM downcore (Fig. 8B). At the core bottom, the V concentration spikes to 664 nM (Fig 7B).

The concentration of pore water Fe in core Geo\_Che4 fluctuates between 3-9 µM downcore to 13 cm, then increases downcore to 16 µM at 19 cm core depth (Fig. 8A). By the core bottom the pore water Fe decreases to <1 µM. The concentration of Mo in the bottom water of core Geo\_Che4 is 158 nM, then increases to 292 nM by 5 cm core depth.

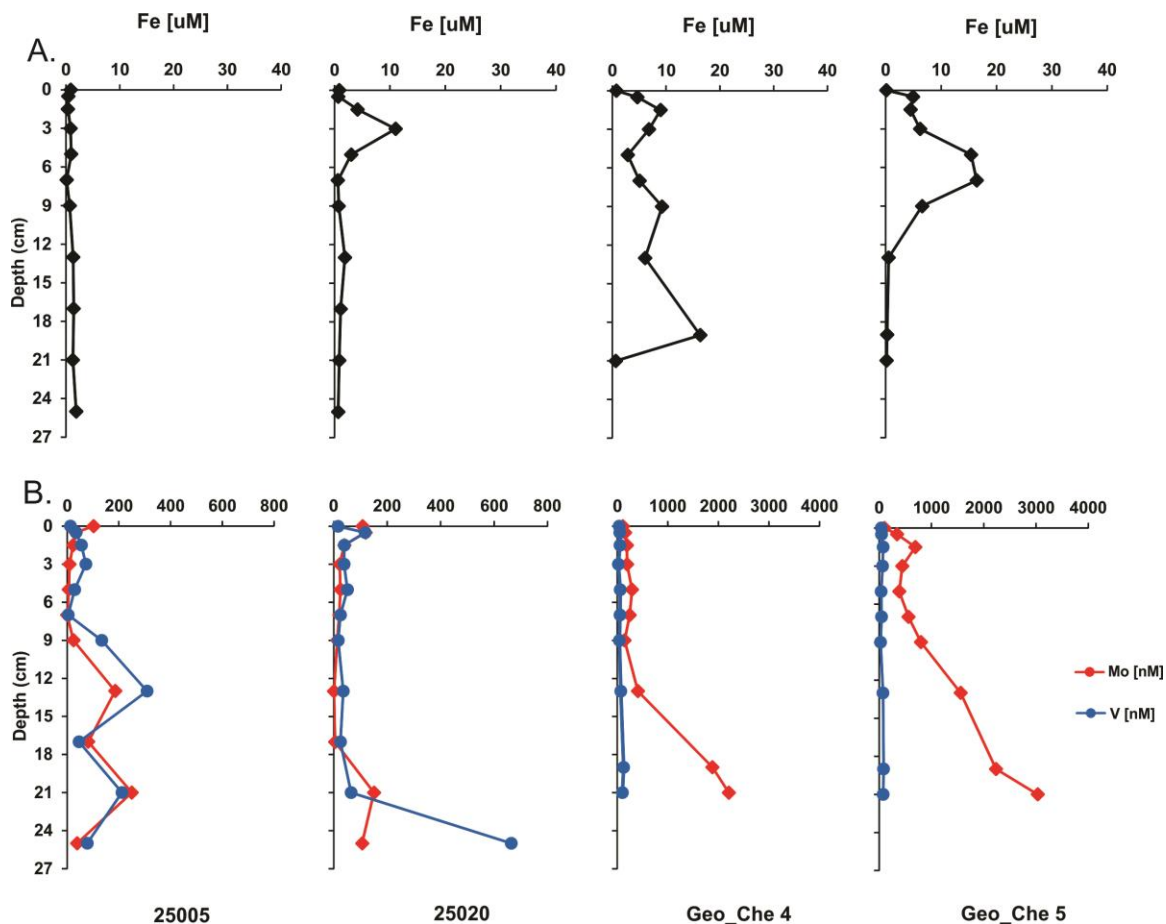


**Figure 8:** Plots of bottom and pore water concentrations of Fe against core depth for cores (from left to right) 25005, 25020, Geo\_Che4, and Geo\_Che5 (A) Plots of Mo (red squares with red line) and V (blue circles with blue line) concentrations against core depth for cores (from left to right) 25005, 25020, Geo\_Che4, and Geo\_Che5 (B).

From 7-9 cm core depth, the Mo concentration decreases to 145 nM, before increasing sharply to 2208 nM by the bottom of the core (Fig. 8B). Dissolved V concentrations are 50 nM in the bottom water and decrease to 22 nM by a core depth of 3 cm, followed by an increase to 58 nM by a core depth of 5 cm, and a decrease to 44 nM by a core depth of 9 cm (Fig. 8B). From 13-19 cm core depth the dissolved V concentration increases to 127 nM before decreasing to 103 nM by the core bottom. The slope sediments from core Geo\_Che5 have a bottom water Fe concentration of  $<1 \mu\text{M}$ , which increases downcore to  $5 \mu\text{M}$  at 3 cm, followed by a spike to  $16 \mu\text{M}$  at 7 cm core depth (Fig. 8A). By the core bottom, the pore water Fe concentration is  $0 \mu\text{M}$ . The concentration

of Mo is 124 nM in the bottom water then immediately increases to 345 nM within the first 0.5 cm of the sediment core (Fig. 8B). The concentration of Mo spikes to 693 nM at a core depth of 1.5 cm, followed by a decrease to 385 nM (at 5 cm core depth) and increases again to 3033 nM at the core bottom. Dissolved V concentrations are 45 nM in the bottom water, 77 nM at 1.5 cm core depth, and decrease to 38 nM by a core depth of 5 cm (Fig. 8B). From 7-9 cm core depth the concentration of V fluctuates before increasing to 83 nM by 19 cm core depth. It is noteworthy to mention that the pore water concentration of V begins to decrease again at the core bottom, which indicates that it is beginning precipitate into the sediment as the environment becomes more reducing.

## CHAPTER FOUR

### DISCUSSION

#### 4.1 REDOX ENVIRONMENTS IN THE STUDY AREA

The shelf sediments, represented by core 25005, are being deposited in an anoxic environment due to high rates of microbial degradation of organic matter rapidly consuming the available upwelled oxygen in the surface water and water column. Evidence for this is seen in the low oxygen concentrations in the bottom water and the enrichment of redox sensitive trace metals (Mo and V; Fig. 6) in the sediment. The absence of solid phase Mn in the shelf sediments (Fig. 5) also reflects the severe oxygen depletion in the shelf bottom waters; Fe and Mn-(oxyhydr)oxide deposits only develop under an oxic water column, so any Mn in the shelf sediments would be dissolved and transported further offshore into more oxic waters (Emerson and Husted, 1991). The absence of laminations in this core may be due to the shallow water depth (49 m) in which sediments are subject to storm wave base disturbances. One other possibility is that the sediments may have been disturbed through the recent attempt to mine for phosphorites in this area.

The laminated mudbelt sediments have the highest TOC, V and Mo contents in the BUS due to the reducing environment (Fig. 5; Fig. 6). Pore water Fe, V, and Mo concentrations are low, confirming that there is dissolved sulfide accumulating in the sediments below 6-7 cm core depth (Fig. 8). As the pore water Fe decreases from the formation of iron sulfides just below the sediment/water interface (SWI), the dissolved sulfide will begin to accumulate in the pore water (Berner, 1970; Raiswell and Canfield, 2012), which causes the V and Mo to precipitate into the sediments, as shown by the increase of solid phase V and Mo concentrations (Fig. 6). The amount



of highly reactive iron phases is not decreasing downcore however (Fig. 4), it is increasing. A higher input of iron in the past into the sediments beneath core 25020 would explain why there is a downcore increase in the highly reactive iron phase. Since the rate of sedimentation for this site is 50-60 cm/kyr (Mollenhauer et al., 2002) our core represents approximately the last 440 years, which is not a long enough time for the complete removal (through iron sulfide formation) of the iron oxy(hydr)oxide phases from the sediments (Raiswell and Canfield, 2012).

The observations of tubes/worms in core Geo\_Che4, low TOC contents (Fig 5), low solid phase Mo contents (Fig. 6), and low solid phase V contents (Fig. 6) indicate that the environment on the shelf break is suboxic. The benthic organisms are bringing dissolved oxygen down into the sediments through bioturbation. The added oxygen causes a decrease in concentration of solid phase V and Mo (Fig. 6) as the redox sensitive metals are oxidized and released into the pore water (Canfield, 1994). The increase in dissolved V and Mo in the pore water is consistent with the oxidation of solid phase V and Mo in the sediments (Fig. 8).

The absence of laminations and the direct measurements of dissolved oxygen in the bottom water of the slope sediments (Table 1) indicate an oxic environment. Sediments in the slope core nevertheless have high TOC contents (Fig. 5) and geochemical signatures (slight V and Mo enrichments (Fig. 6)) that could represent a more reducing redox environment. These enrichments can be explained by the high rates of sedimentation on the slope (Mollenhauer et al., 2002). Pore water profiles of dissolved Fe are decreasing at 13 cm core depth (Fig. 8), which indicates reducing conditions re-occur at this depth, as shown by the increasing dissolved pore water V and Mo concentrations. The bioturbation occurring at this location provides oxygen to the upper sediments, which also contributes to the increase of dissolved V and Mo in the pore water (Fig. 8) from the re-oxidation of authigenic metal phases that were precipitated during reducing periods. Because the concentration of dissolved sulfides in the bottom half of the core must not be high

enough to activate the geochemical switch for Mo precipitation ( $>100 \mu\text{M}$ ), the dissolved Mo accumulates in the pore water.

The interpretations of ancient environments in which black shales are deposited have been based on observations in modern environments where organic matter presently accumulates: ocean upwelling areas (e.g., the Benguella upwelling) and restricted basins (e.g., the Black Sea; Higginson, 2009). Understanding the chemical processes of the water column and pore water in modern environments helps us to decipher the controls on the deposition of ancient organic rich deposits (Piper and Calvert, 2009). One method that has been used to decipher bottom water redox state in ancient black shale deposits is the ratio of V/Mo (Emerson and Husted, 1991; Piper and Calvert, 2009). If a shale was deposited under anoxic conditions, the V/Mo ratio should approach the value for average seawater (1.810); if the depositional environment was suboxic, the V/Mo ratio will be elevated (Piper and Calvert, 2009). Plots of V/Mo in this modern analogue of black shale formation, cores 25005, 25020, Geo\_Che4, and Geo\_Che5, are shown in Figure 9. The pink stripe marks the range in which sediments were deposited in anoxic bottom water, while data plotting on the right side of the stripe represents deposition under suboxic bottom water conditions. This proxy for black shale depositional environment does accurately describe the data from this study, in that the only core deposited under anoxic conditions in the Benguela Upwelling System is core 25020 from the shelf mudbelt. Core Geo\_Che4 and Geo\_Che5, deposited respectively in suboxic and oxic redox environments, can also be accurately described by the V/Mo relationship.

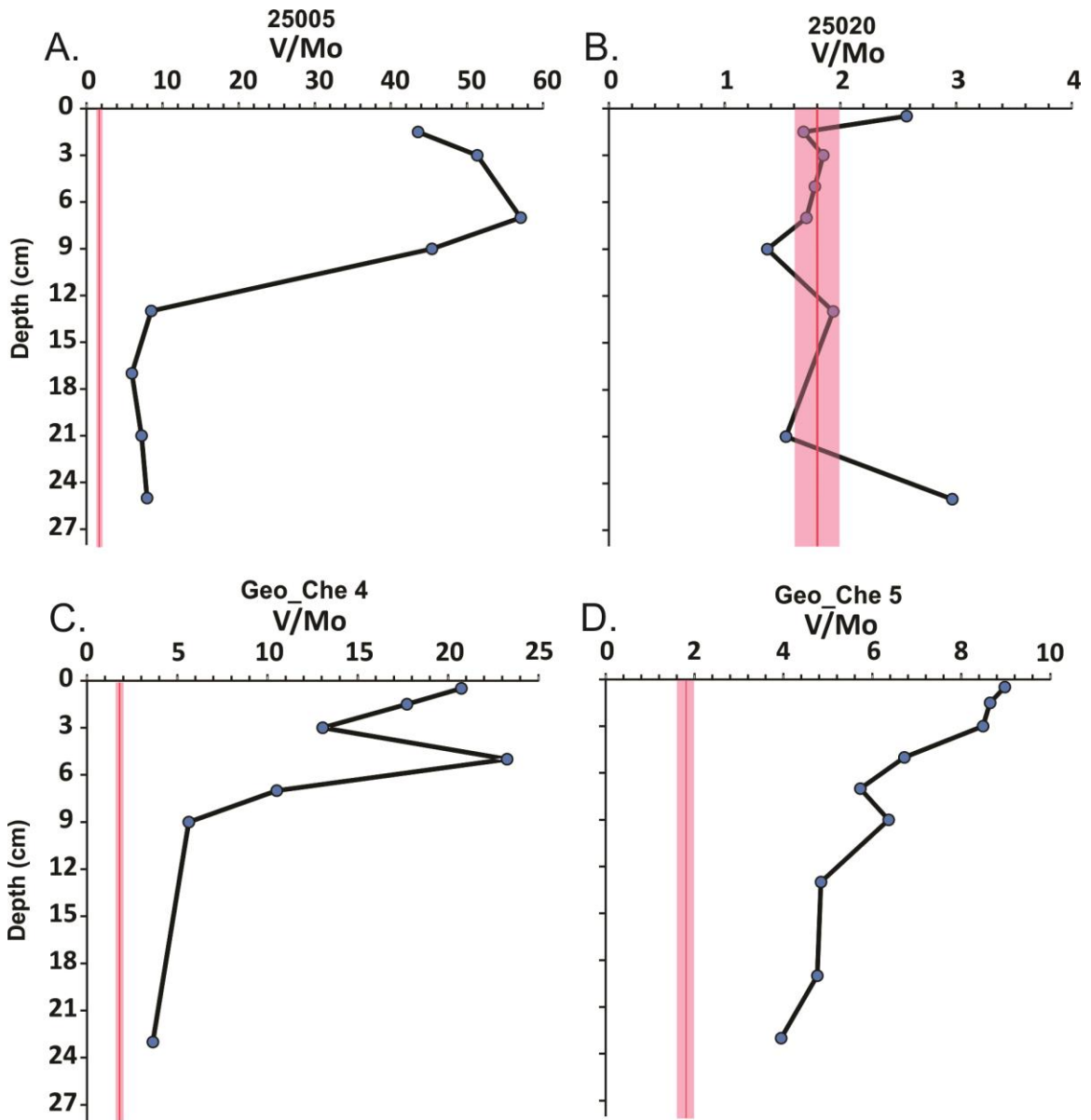


**Figure: 9:** V/Mo relationship vs. core depth for cores 25005, 25020, Geo\_Che4, and Geo\_Che5. The area shaded in pink represents the zone in which sediments were deposited under fully anoxic conditions in the bottom water. Points that fall to the right side of this zone represent deposition in suboxic bottom water conditions.

#### 4.2 NI/TOC RATIOS IN UPWELLING ZONES AND REDEPOSITION

In a recent study, combined data from short cores obtained from Peru, Gulf of California, Chile, and the Benguela Upwelling System were used to show that organic-rich sediments from upwelling zones have a linear Ni/TOC relationship (Böning et al., 2015). A plot of the Ni and TOC data from this study, using the same scale as the Böning et al. (2015) study, reveals a similar linearity in the sediments from the shelf mudbelt (25020) core (Fig. 10).

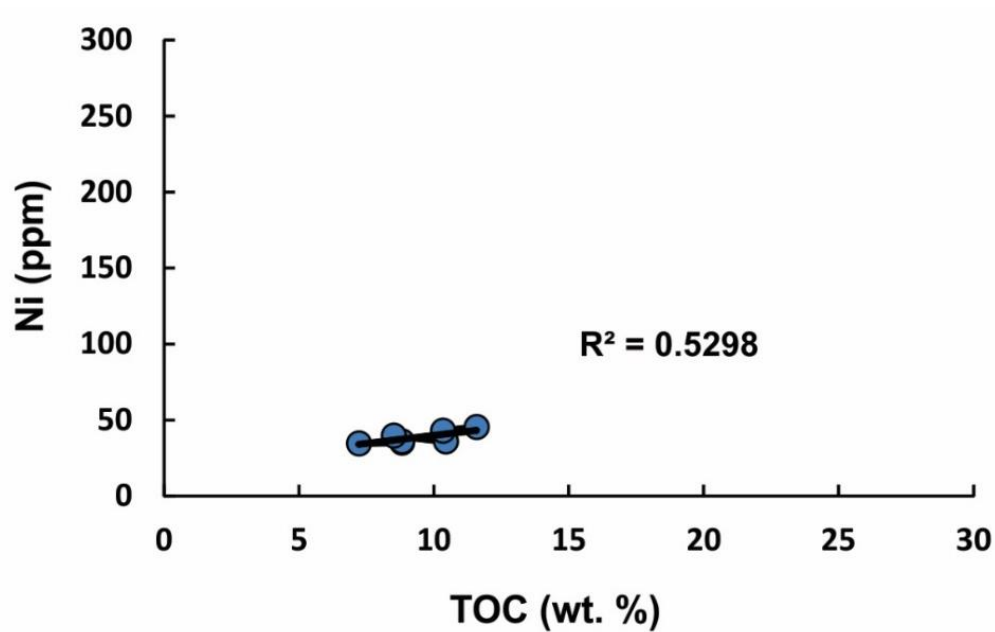


**Figure 10:** The nickel (Ni) to total organic carbon (TOC) cross plot for shelf sediments (core 25020) from the Benguela Upwelling System.

However, the linear relationship does not remain, as seen in the plot of the Ni/TOC relationship for the sediments on the slope (core Geo\_Che5) (Fig. 11). The shelf mudbelt is the source of the organic matter and sediments presently accumulating on the slope depocenter from lateral (offshore) sediment transport in nepheloid layers (Inthorn et al., 2006a).

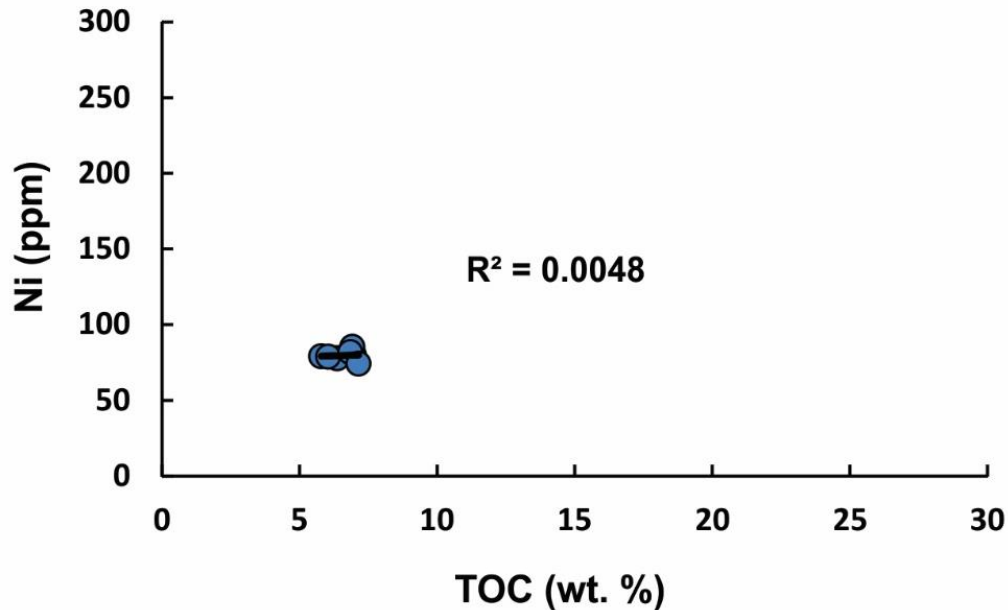


**Figure 11:** The nickel (Ni) to total organic carbon (TOC) cross plot, shown as blue circles, for slope sediments (core Geo\_Che5) from the Benguela Upwelling System. No linear correlation can be observed, however, there are very few data points to consider.

Some of the OM on the slope is being remineralized by the available oxygen in the bottom water, or possibly while in transit within the nepheloid layers; and this is observed in the slightly lower TOC content for the slope core (Fig. 5D). The shelf edge upwelling, which spawns additional productivity over the slope, adds additional Ni (Fig. 6D) to the slope that is delivered to the sediment with the sinking OM found in the waters above. When the sinking OM encounters the oxygen in the waters immediately below the OMZ, a portion of the organic matter is remineralized while the Ni remains in the sediment. The non-linear relationship seen in the sediments in core Geo\_Che5 (Fig. 11) is the expected result in this type of an environment. A plot of the mudbelt core (25020) and the slope depocenter core (Geo\_Che5) is superimposed onto the figure from the Böning et al. (2015) study (Fig. 12) to highlight the linearity of the shelf core and the non-linear relationship occurring on the slope.

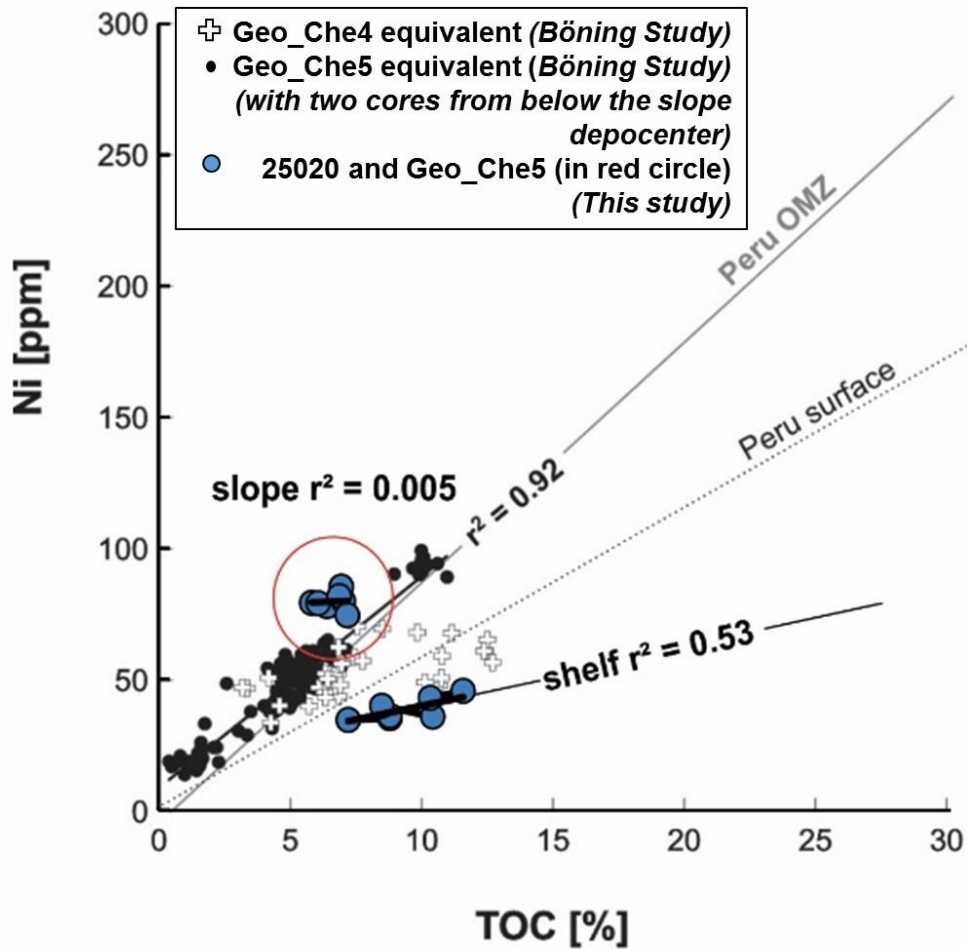


**Figure 12:** Plots of the Namibian shelf core sediments (25020, blue circles) and slope sediments (Geo\_Che5, blue circles enclosed by the red circle) superimposed on the figure from (Böning et al., 2015) that shows the linear relationship between nickel (Ni) and total organic carbon (TOC) from the Benguela Upwelling System compared to the regression line from the Ni/TOC relationship in the Peru upwelling system. Note that there is an  $r^2$  value of 0.005 for the slope sediments from the Benguela Upwelling System due to the redeposition of the sediments by lateral transport changing the linear relationship.

The information from the Böning et al. (2015) study demonstrates that in upwelling zone sediments, Ni/TOC is positively correlated. Therefore, the Ni/TOC relationship found on the slope from this study must demonstrate that the geochemical signature for redeposition begins with a Ni/TOC relationship that is not linear. It has been established that the shelf mudbelt and slope depocenter in the Namibian coast are two environments of organic carbon preservation that represent an environment of original deposition and redeposition beneath an upwelling OMZ

(Inthorn et al., 2006a). The sediments from the shelf mudbelt (core 25020) are the primary deposited upwelling sediments, while the sediments from the slope core (Geo\_Che5) have been redeposited (Inthorn et al., 2006b). A linear relationship does exist between Ni and TOC in core 25020 (Figure 10). Thus, we propose that this non-linear Ni/TOC ratio, when combined with the enrichments of Mo and V and the bioturbation structures, can be used as a tool to identify redepositional settings from an upwelling oxygen minimum zone if found in an ancient rock.

The reconstruction of paleo-redox conditions and paleo-depositional environments in black shales is sometimes compromised due to the discrepancies between geochemical and sedimentological proxies (Schieber, 2001). A study by Schieber (2001) revealed that bioturbation structures were found in black shales that were geochemically determined to be deposited in an anoxic setting. One explanation that this study from the Benguela Upwelling System can offer is that these shales were originally deposited in an anoxic setting, such as the sediments from core 25020 (shelf mudbelt), followed by redeposition into an oxic environment, such as the sediments from core Geo\_Che5 on the slope. Some of the original authigenic V and Mo that precipitated while on the shelf must have remained in the redeposited sediments and was measured in core Geo\_Che5 (Fig. 6D). The redox environment beneath the oxic sediment/water interface then became reducing again due to the microbial degradation of the large amounts of organic matter present. A black shale that was deposited in this type of environment would contain all of the features, both geochemical and sedimentological, of core Geo\_Che5, including bioturbation marks and enrichments V and Mo. One method in which to test this hypothesis would be to examine the Ni/TOC relationship for the shale in question. If there is no positive correlation, the shale may have been the result of lateral transport and redeposition within an ocean upwelling oxygen minimum zone.

## CHAPTER FIVE

### SUMMARY AND CONCLUSION

Organic rich sediments from four sites in the Benguela Upwelling System were examined for pore water and solid phase geochemistry. In summary, with the exception of the shelf mudbelt area, the geochemical properties of the organic rich sediments in this system show that deposition is taking place under anoxic, suboxic, and oxic conditions in the bottom water. The trace metals that are usually associated with deposition of sediments under anoxic or sulfidic conditions, mainly V and Mo, are enriched in the surface sediments of this system regardless of the presence of oxygen in the bottom water, although redox sensitive metals display highest enrichments in the anoxic settings. The enrichment of redox sensitive trace metals, Mo and V, must therefore not only occur in anoxic and sulfidic sediments.

In this study, the redox environment of the bottom water and the surface sediments were first constrained using results from both aqueous and solid phase V and Mo contents and iron phase data. Our results show that the organic rich mudbelt on the shelf is the only area with anoxic conditions in the bottom water. The data also shows that the redox environment on the shelf break and the upper slope is suboxic to oxic yet there are still large amounts of organic carbon being preserved in the surface sediments. The ratio of V/Mo, a proxy that has been used to determine the paleo-redox environment of the bottom water during black shale deposition, was also analyzed as a way of re-confirming our results, while at the same time confirming the accuracy of the proxy with a modern analogue for black shale deposition. The results of the V/Mo ratios from this study also agree that there is only one area in this system that is preserving organic carbon to the sediments under anoxic bottom water conditions. Our data also confirms the validity of this proxy used to determine the bottom water redox conditions of black shale deposition.



Ni/TOC in upwelling systems have recently been found to show a positive correlation (Böning et al., 2015). The shelf mudbelt from the Benguela Upwelling system shows this linear relationship in the anoxic sediments from core 25020. However, this system is transporting the anoxic and organic carbon rich sediments from the shelf to a second, more oxic area of redeposition on the upper slope. Our findings show that the relationship between Ni and TOC is not correlative in the slope sediments, due to partial oxidation of the organic matter while being transported and redeposited into increasingly oxic waters. High sedimentation rates on the slope, and therefore quick burial, allows for the preservation of the remaining organic matter in the slope depocenter. This non-correlative Ni/TOC relationship of the redeposited sediments becomes the signal that is then recorded in the geological record.

Combining all of these characteristics, the enrichment of Mo and V in organic-rich sediments deposited in suboxic or oxic conditions and a non-correlative relationship between Ni and TOC, with sedimentological features observed such as bioturbation structures, we can see the geochemical signature for a redepositional setting from an upwelling oxygen minimum zone. The geochemical signature of a redepositional system will be a useful tool for identifying environments of organic carbon redeposition beneath upwelling oxygen minimum zones that are recorded in ancient black shales. Additionally, being able to recognize areas of redeposition in black shales may also solve some of the unanswered questions remaining about shales that display the markings of bioturbation, and at the same time, contain the geochemical signatures for anoxic deposition. Future work for this study could include the analysis of Mo, V, Ni, and TOC in some of the bioturbated sections found in the Woodford Shale, the Antrim Shale, the New Albany Shale, and the Cleveland Shale. Additionally, it would be of interest to analyze deeper sediment from beneath the cores in this study in order to observe how the Ni/TOC ratio changes downcore through lithification and further diagenesis.

All ocean upwelling systems do not undergo intense lateral redeposition processes to the extent that it is occurring in the Benguela Upwelling System. However, the principal of uniformitarianism dictates that a more complete understanding of the geochemical controls on organic carbon-rich deposits from modern sediments will help us to better understand the geochemical controls on ancient organic-rich deposits.

## REFERENCES

- Algeo, T., and Lyons, T. (2006). Mo–total organic carbon covariation in modern anoxic marine environments: Implications for analysis of paleoredox and paleohydrographic conditions. *Paleoceanography*, 21(1).
- Algeo, T., and Maynard, J. (2004). Trace-element behavior and redox facies in core shales of Upper Pennsylvanian Kansas-type cyclothems. *Chemical Geology*, 206(3), 289-318.
- Algeo, T., and Rowe, H. (2012). Paleoceanographic applications of trace-metal concentration data. *Chemical Geology*, 324, 6-18.
- Allen, J., and Thornley, D. (2004). Laser granulometry of Holocene estuarine silts: effects of hydrogen peroxide treatment. *The Holocene*, 14(2), 290-295.
- Álvarez-Iglesias, P., and Rubio, B. (2009). Redox status and heavy metal risk in intertidal sediments in NW Spain as inferred from the degrees of pyritization of iron and trace elements. *Marine Pollution Bulletin*, 58(4), 542-551.
- Berger, W., and Wefer, G. (2002). On the reconstruction of upwelling history: Namibia upwelling in context. *Marine Geology*, 180(1), 3-28.
- Berner, R. (1970). Sedimentary pyrite formation. *American Journal of Science*, 268(1), 1-23.
- Böning, P., Shaw, T., Pahnke, K., and Brumsack, H. (2015). Nickel as indicator of fresh organic matter in upwelling sediments. *Geochimica et Cosmochimica Acta*, 162, 99-108.
- Böning, P., Fröllje, H., Beck, M., Schnetger, B., and Brumsack, H. (2012). Underestimation of the authigenic fraction of Cu and Ni in organic-rich sediments. *Marine Geology*, 323, 24-28.
- Borchers, S., Schnetger, B., Böning, P., and Brumsack, H. (2005). Geochemical signatures of the Namibian diatom belt: Perennial upwelling and intermittent anoxia. *Geochemistry, Geophysics, Geosystems*, 6(6).
- Brongersma-Sanders, M., Stephan, K., Kwee, T., and De Bruin, M. (1980). Distribution of minor elements in cores from the Southwest Africa shelf with notes on plankton and fish mortality. *Marine Geology*, 37(1-2), 91-132.
- Brumsack, H. (1989). Geochemistry of recent TOC-rich sediments from the Gulf of California and the Black Sea. *Geologische Rundschau*, 78(3), 851-882.
- Brumsack, H. (2006). The trace metal content of recent organic carbon-rich sediments: implications for Cretaceous black shale formation. *Palaeogeography, Palaeoclimatology, Palaeoecology*, 232(2), 344-361.
- Callot, H., Ocampo, R., and Albrecht, P. (1990). Sedimentary porphyrins: correlations with biological precursors. *Energy and Fuels*, 4(6), 635-639.
- Calvert, S., and Pedersen, T. (1992). Organic carbon accumulation and preservation in marine sediments: how important is anoxia. *Organic matter: productivity, accumulation, and preservation in recent and ancient sediments*, 533, 231-263.

- Calvert, S. and Price, N. (1983). Geochemistry of Namibian shelf sediments. In *Coastal Upwelling Its Sediment Record* (pp. 337-375). Springer US.
- Canfield, D. E. (1994). Factors influencing organic carbon preservation in marine sediments. *Chemical Geology*, 114(3), 315-329.
- Carr, M. E. (2002). Estimation of potential productivity in eastern boundary currents using remote sensing. *Deep Sea Research, (Part II)*, 59, 80.
- Cruse, A and Lyons, T. (2004). Trace metal records of regional paleoenvironmental variability in Pennsylvanian (Upper Carboniferous) black shales. *Chemical Geology*, 206(3), 319-345.
- Crusius, J., Calvert, S., Pedersen, T., and Sage, D. (1996). Rhenium and molybdenum enrichments in sediments as indicators of oxic, suboxic and sulfidic conditions of deposition. *Earth and Planetary Science Letters*, 145(1), 65-78.
- DeMaster, D. (1981). The supply and accumulation of silica in the marine environment. *Geochimica et Cosmochimica acta*, 45(10), 1715-1732.
- Emerson, S., and Husted, S. (1991). Ocean anoxia and the concentrations of molybdenum and vanadium in seawater. *Marine Chemistry*, 34(3), 177-196.
- Giraudeau, J., Monteiro, P., and Nikodemus, K. (1993). Distribution and malformation of living coccolithophores in the northern Benguela upwelling system off Namibia. *Marine Micropaleontology*, 22(1), 93-110.
- Helz, G., Miller, C., Charnock, J., Mosselmans, J., Patrick, R., Garner, C., and Vaughan, D. (1996). Mechanism of molybdenum removal from the sea and its concentration in black shales: EXAFS evidence. *Geochimica et Cosmochimica Acta*, 60(19), 3631-3642.
- Higginson, M. (2009). Geochemical Proxies (Non-Isotopic). In *Encyclopedia of Paleoclimatology and Ancient Environments* (pp. 341-354). Springer Netherlands.
- Inthorn, M., Mohrholz, V., and Zabel, M. (2006a). Nepheloid layer distribution in the Benguela upwelling area offshore Namibia. *Deep Sea Research Part I: Oceanographic Research Papers*, 53(8), 1423-1438.
- Inthorn, M., Wagner, T., Scheeder, G., and Zabel, M., (2006b). Lateral transport controls distribution, quality, and burial of organic matter along continental slopes in high-productivity areas. *Geology*, 34 no. 3, 205-208.
- Jacobs, L., Emerson, S., and Skei, J. (1985). Partitioning and transport of metals across the O<sub>2</sub> H<sub>2</sub>S interface in a permanently anoxic basin: Framvaren Fjord, Norway. *Geochimica et Cosmochimica Acta*, 49(6), 1433-1444.
- Krishnamurthy, R., Atekwana, E., and Guha, H. (1997). A simple, inexpensive carbonate-phosphoric acid reaction method for the analysis of carbon and oxygen isotopes of carbonates. *Analytical Chemistry*, 69(20), 4256-4258.
- Kunze, G. and Dixon, J. (1986). Pretreatment for mineralogical analysis. *Methods of Soil Analysis: Part 1—Physical and Mineralogical Methods, (methods of soil analysis 1)*, 91-100.
- Lipinski, M., Warning, B., and Brumsack, H. J. (2003). Trace metal signatures of Jurassic/Cretaceous black shales from the Norwegian Shelf and the Barents Sea. *Palaeogeography, Palaeoclimatology, Palaeoecology*, 190, 459-475.

- Lutjeharms, J. and Meeuwis, J. (1987). The extent and variability of South-East Atlantic upwelling. *South African Journal of Marine Science*, 5(1), 51-62.
- Martin, J., and Knauer, G. (1973). The elemental composition of plankton. *Geochimica et Cosmochimica Acta*, 37(7), 1639-1653.
- McLennan, S. (2001). Relationships between the trace element composition of sedimentary rocks and upper continental crust. *Geochemistry, Geophysics, Geosystems*, 2(4).
- Mollenhauer, G., Schneider, R. R., Müller, P. J., Spieß, V., & Wefer, G. (2002). Glacial/interglacial variability in the Benguela upwelling system: Spatial distribution and budgets of organic carbon accumulation. *Global Biogeochemical Cycles*, 16(4).
- Mollenhauer, G., Inthorn, M., Vogt, T., Zabel, M., Damsté, J., and Eglinton, T. (2007). Aging of marine organic matter during cross-shelf lateral transport in the Benguela upwelling system revealed by compound-specific radiocarbon dating. *Geochemistry, Geophysics, Geosystems*, 8(9).
- Morse, J., and Luther, G. (1999). Chemical influences on trace metal-sulfide interactions in anoxic sediments. *Geochimica et Cosmochimica Acta*, 63(19), 3373-3378.
- Müller, P., and Suess, E. (1979). Productivity, sedimentation rate, and sedimentary organic matter in the oceans—I. Organic carbon preservation. *Deep Sea Research Part A. Oceanographic Research Papers*, 26(12), 1347-1362.
- Nameroff, T., Balistrieri, L., and Murray, J. (2002). Suboxic trace metal geochemistry in the eastern tropical North Pacific. *Geochimica et Cosmochimica Acta*, 66(7), 1139-1158.
- Pedersen, T., and Calvert, S. (1990). Anoxia vs. productivity: what controls the formation of organic-carbon-rich sediments and sedimentary Rocks?(1). *AAPG Bulletin*, 74(4), 454-466.
- Philander, S., and Yoon, J. (1982). Eastern boundary currents and coastal upwelling. *Journal of Physical Oceanography*, 12(8), 862-879.
- Piper, D., and Calvert, S. (2009). A marine biogeochemical perspective on black shale deposition. *Earth-Science Reviews*, 95(1), 63-96.
- Pitcher, G., Walker, D., Mitchell-Innes, B., and Moloney, C. (1991). Short-term variability during an anchor station study in the southern Benguela upwelling system: phytoplankton dynamics. *Progress in Oceanography*, 28(1), 39-64.
- Poulton, S., and Canfield, D. (2005). Development of a sequential extraction procedure for iron: implications for iron partitioning in continentally derived particulates. *Chemical Geology*, 214(3), 209-221.
- Raiswell, R., Vu, H., Brinza, L., and Benning, L. (2010). The determination of labile Fe in ferrihydrite by ascorbic acid extraction: Methodology, dissolution kinetics and loss of solubility with age and de-watering. *Chemical Geology* 70-79.
- Raiswell, R., Canfield, D., Berner, R., (1994). A comparison of iron extraction methods for the determination of degree of pyritization and the recognition of iron-limited pyrite formation. *Chem. Geol.* 111, 101–110.
- Raiswell, R., and Canfield, D. (1998). Sources of iron for pyrite formation in marine sediments. *American Journal of Science*, 298(3), 219-245.

- Raiswell, R., and Canfield, D. (2012). The iron biogeochemical cycle past and present. *Geochemical Perspectives*, 1(1), 1-2.
- Riedinger, N., Kasten, S., Gröger, J., Franke, C., and Pfeifer, K. (2006). Active and buried authigenic barite fronts in sediments from the Eastern Cape Basin. *Earth and Planetary Science Letters*, 241(3), 876-887.
- Robinson, R., Meyers, P., and Murray, R. (2002). Geochemical evidence for variations in delivery and deposition of sediment in Pleistocene light–dark color cycles under the Benguela Current Upwelling System. *Marine Geology*, 180(1), 249-270.
- Schieber, J. (2001). A role for organic petrology in integrated studies of mudrocks: examples from Devonian black shales of the eastern US. *International journal of coal geology*, 47(3), 171-187.
- Schieber, J. (2009). Discovery of agglutinated benthic foraminifera in Devonian black shales and their relevance for the redox state of ancient seas. *Palaeogeography, Palaeoclimatology, Palaeoecology*, 271(3), 292-300.
- Schmidt, M., and Eggert, A. (2012). A regional 3D coupled ecosystem model of the Benguela upwelling system. Leibniz-Institut für Ostseeforschung Warnemünde. *Marine Science Reports*. No. 87.
- Scholz, F., Hensen, C., Noffke, A., Rohde, A., Liebetrau, V., and Wallmann, K. (2011). Early diagenesis of redox-sensitive trace metals in the Peru upwelling area—response to ENSO-related oxygen fluctuations in the water column. *Geochimica et Cosmochimica Acta*, 75(22), 7257-7276.
- Scott, C. and Lyons, T. (2012). Contrasting molybdenum cycling and isotopic properties in euxinic versus non-euxinic sediments and sedimentary rocks: Refining the paleoproxies. *Chemical Geology*, 324-325, 19-27.
- Seeborg-Elverfeldt, J., Schlüter, M., Feseker, T., and Kölling, M. (2005). Rhizon sampling of pore waters near the sediment/water interface of aquatic systems. *Limnology and oceanography: Methods*, 3(8), 361-371.
- Shannon, L. (1985). The Benguela ecosystem. I: Evolution of the Benguela physical features and processes. *Oceanography and Marine Biology*, 23, 105-182.
- Shannon, L. and Nelson, G. (1996). The Benguela: large scale features and processes and system variability. In *The South Atlantic* (pp. 163-210). Springer Berlin Heidelberg.
- Shillington, F., Hutchings, L., Probyn, T., Waldron, H., and Peterson, W. (1992). Filaments and the Benguela frontal zone: offshore advection or recirculating loops?. *South African Journal of Marine Science*, 12(1), 207-218.
- Shimmield, G. and Price, N. (1986). The behavior of molybdenum and manganese during early sediment diagenesis—offshore Baja California, Mexico. *Marine Chemistry*, 19(3), 261-280.
- Skogen, M. (2004). A direct estimate of the Namibian upwelling flux. *Namibia's Fisheries: Ecological, Economic and Social Aspects*, 11-28.
- Stookey, L. (1970). Ferrozine---a new spectrophotometric reagent for iron. *Analytical chemistry*, 42(7), 779-781.

- Summerhayes, C., Kroon, D., Rosell-Melé, A., Jordan, R., Schrader, H., Hearn, J., Villanueva, J., Grimalt, G., and Eglinton, G. (1995). Variability in the Benguela Current upwelling system over the past 70,000 years. *Progress in Oceanography*, 35(3), 207-251.
- Tessier, A., Campbell, P., and Bisson, M. (1979). Sequential extraction procedure for the speciation of particulate trace metals. *Analytical chemistry*, 51(7), 844-851.
- Tribovillard, N., Algeo, T., Lyons, T., and Riboulleau, A. (2006). Trace metals as paleoredox and paleoproductivity proxies: an update. *Chemical Geology*, 232(1), 12-32.
- Twining, B., Baines, S., Vogt, S., and Nelson, D. (2012). Role of diatoms in nickel biogeochemistry in the ocean. *Global Biogeochemical Cycles*, 26(4).
- Viollier, E., Inglett, P., Hunter, K., Roychoudhury, A., and Van Cappellen, P. (2000). The ferrozine method revisited: Fe (II)/Fe (III) determination in natural waters. *Applied Geochemistry*, 15(6), 785-790.
- Wilde, P., Lyons, T., and Quinby-Hunt, M. (2004). Organic carbon proxies in black shales: molybdenum. *Chemical Geology*, 206(3), 167-176.
- Wilson, S., and Weber, J. (1979). An EPR study of the reduction of vanadium (V) to vanadium (IV) by fulvic acid. *Chemical Geology*, 26(3), 345-354.

SUPPLEMENTARY DATA

**Table S1:** Iron phase results for solid phase iron extractions related to carbonate forming (Fe<sub>CARB</sub>), iron oxide forming (Fe<sub>OXIDES</sub>), and magnetite forming (Fe<sub>MAG</sub>) iron phases in sediments from cores 25005, 25020, Geo\_Che4, and Geo\_Che5.

Core	Depth (cm)	Water %	Fe <sub>CARB</sub> (mg/kg)	Fe <sub>OXIDES</sub> (mg/kg)	Fe <sub>MAG</sub> (mg/kg)
<b>25005</b>	1	38	555	402	325
	2	50	474	387	343
	3	44	459	360	310
	5	37	372	325	288
	7	36	382	354	322
	9	33	226	381	333
	13	64	300	276	418
	17	66	180	215	430
	21	61	152	308	445
	<b>25020</b>	25	63	77	148
1		90	484	523	313
2		86	227	419	277
3		85	232	654	257
5		82	254	429	337
7		80	380	479	403
9		80	119	685	425
13		82	186	767	633
17		78	92	1069	1096
21		71	5	1187	1454
<b>Geo_Che4</b>	25	66	3	1302	1589
	1	46	161	370	199
	2	46	25	438	183
	3	46	22	333	192
	5	40	35	302	189
	7	40	33	258	187
	9	45	22	187	181
	13	42	-	250	207
	19	36	-	146	192
	<b>Geo_Che5</b>	23	37	-	147
1		66	96	805	304
2		67	212	708	209
3		66	82	511	224
5		68	404	859	292
7		67	159	710	247
9		65	312	876	213
13		66	38	366	223
19		62	118	641	245
23		63	13	341	216

- = below detection limit



**Table S2:** Solid phase TOC, CaCO<sub>3</sub>, Al, Mn, Fe, Fe<sub>HR</sub>, V, Mo, and Ni for cores 25005, 25020, Geo\_Che4, and Geo\_Che5.

Core	Core Depth (cm)	TOC (wt %)	CaCO <sub>3</sub> (wt %)	Al (wt%)	Mn (mg/kg)	Fe (wt%)	Fe <sub>(HR)</sub> (mg/kg)	V (mg/kg)	Mo (mg/kg)	Ni (mg/kg)
<b>25005</b>	0.5	1.1	1.8	3.59	557.41	2.96	1282	130.42	0.35	33.01
	1.5	2.6	2.5	3.24	348.91	2.30	1204	92.95	2.13	31.52
	3.0	2.4	1.7	3.43	456.22	2.67	1129	111.73	2.18	33.54
	5.0	1.6	-	-	-	-	985	-	-	-
	7.0	1.8	2.2	3.36	518.42	2.86	1057	123.60	2.17	33.18
	9.0	1.5	2.0	3.30	523.51	2.74	940	119.67	2.64	32.82
	13.0	3.6	2.3	3.38	249.83	2.24	996	74.51	8.77	38.36
	17.0	4.3	5.8	3.83	215.23	2.38	826	71.63	12.03	46.03
	21.0	4.4	5.8	2.95	123.31	1.96	904	51.13	7.07	143.26
25.0	4.0	6.3	3.84	197.59	2.27	624	63.46	7.98	42.73	
<b>25020</b>	0.5	7.8	17.1	0.87	38.03	0.62	1321	47.06	18.30	31.41
	1.5	8.7	13.2	1.24	56.46	0.85	923	37.18	22.09	43.75
	3.0	7.2	17.4	1.29	61.41	0.92	1143	38.02	20.54	44.25
	5.0	8.8	10.8	1.36	62.59	0.96	1020	39.84	22.38	47.87
	7.0	8.8	7.2	1.28	60.84	0.94	1262	41.64	24.40	46.05
	9.0	8.5	9.2	3.63	168.66	2.77	1229	92.07	67.27	144.44
	13.0	10.4	11.0	1.86	86.52	1.33	1585	49.85	25.72	66.62
	17.0	10.3	8.0	-	-	-	2257	-	-	-
	21.0	10.3	10.6	2.11	93.40	1.62	2646	62.11	40.60	90.49
25.0	11.6	11.1	3.18	159.74	2.56	2894	199.28	67.17	144.68	
<b>Geo_Che4</b>	0.5	3.3	26.5	1.38	82.47	1.44	730	30.78	3.43	53.03
	1.5	3.4	35.3	1.04	65.10	1.22	646	25.63	2.96	44.40
	3.0	3.2	36.1	1.25	88.07	1.50	547	32.58	3.84	54.45
	5.0	3.8	28.1	1.29	92.49	1.66	526	33.58	5.00	52.87
	7.0	3.1	33.1	1.00	72.63	1.44	479	29.88	5.22	51.94
	9.0	3.3	35.2	1.23	82.75	1.53	390	31.65	4.97	53.02
	13.0	3.1	22.8	1.05	76.78	1.37	453	31.26	6.45	59.03
	19.0	3.1	28.6	1.24	80.33	1.57	330	32.95	6.92	53.51
	23.0	2.5	30.0	1.25	81.81	1.46	334	32.10	8.14	56.43
<b>Geo_Che5</b>	0.5	5.8	50.5	1.68	66.13	1.06	1109	26.61	1.28	79.23
	1.5	6.4	49.5	1.66	65.82	1.04	917	26.16	1.48	77.97
	3.0	6.0	40.8	1.60	67.41	1.07	735	27.58	2.11	79.03
	5.0	7.0	54.2	1.67	68.70	1.10	1151	27.04	1.16	79.92
	7.0	6.9	50.6	1.43	72.78	1.20	957	28.55	2.72	85.40
	9.0	6.8	-	1.62	67.95	1.11	1089	26.70	4.74	81.80
	13.0	7.7	34.8	1.70	78.50	1.40	589	33.70	6.20	47.00
	19.0	7.4	63.0	1.40	66.80	1.20	886	31.60	7.50	35.20
	23.0	7.1	43.1	1.60	61.52	1.01	557	26.75	7.33	74.44

- = not measured

**Table S3:** Bottom water (0 cm) and pore water Fe, Mo, and V concentrations from cores 25005, 25020, Geo\_Che4, and Geo\_Che5.

Core	Core Depth (cm)	Fe $\mu\text{M}$	Mo nM	V nM
<b>25005</b>	0	0.88	102.15	12.41
	0.5	0.42	33.48	34.55
	1.5	0.36	22.93	55.18
	3.0	0.83	9.38	72.78
	5.0	0.96	6.35	29.27
	7.0	0.11	-	3.94
	9.0	0.69	24.36	134.01
	13.0	1.33	186.08	309.50
	17.0	1.43	81.73	45.97
	21.0	1.27	249.93	212.46
	25.0	1.90	38.87	77.95
<b>25020</b>	0	0.85	107.69	16.18
	0.5	0.69	119.52	117.30
	1.5	4.17	39.56	39.11
	3.0	11.03	22.29	38.29
	5.0	3.01	25.19	50.97
	7.0	0.61	20.74	24.99
	9.0	0.76	13.25	16.55
	13.0	1.89	0.91	35.34
	17.0	1.12	5.04	25.25
	21.0	0.86	150.59	64.59
	25.0	0.67	106.43	664.25
<b>Geo_Che4</b>	0	0.77	111.52	38.25
	0.5	4.65	157.49	49.78
	1.5	8.97	189.91	53.73
	3.0	6.83	194.51	22.05
	5.0	2.87	291.68	57.77
	7.0	5.08	246.35	53.99
	9.0	9.26	144.83	44.31
	13.0	6.09	408.90	72.37
	19.0	16.36	1883.61	127.21
	23.0	0.67	2208.17	102.85
	<b>Geo_Che5</b>	0	0.22	123.45
0.5		4.93	345.18	44.74
1.5		4.48	692.99	76.85
3.0		6.21	441.91	64.90
5.0		15.41	384.78	37.94
7.0		16.42	562.34	47.43
9.0		6.56	800.55	25.41
13.0		0.52	1560.65	72.06
19.0		0.26	2236.06	83.18
23.0		0.16	3033.26	77.94

- = below detection limit

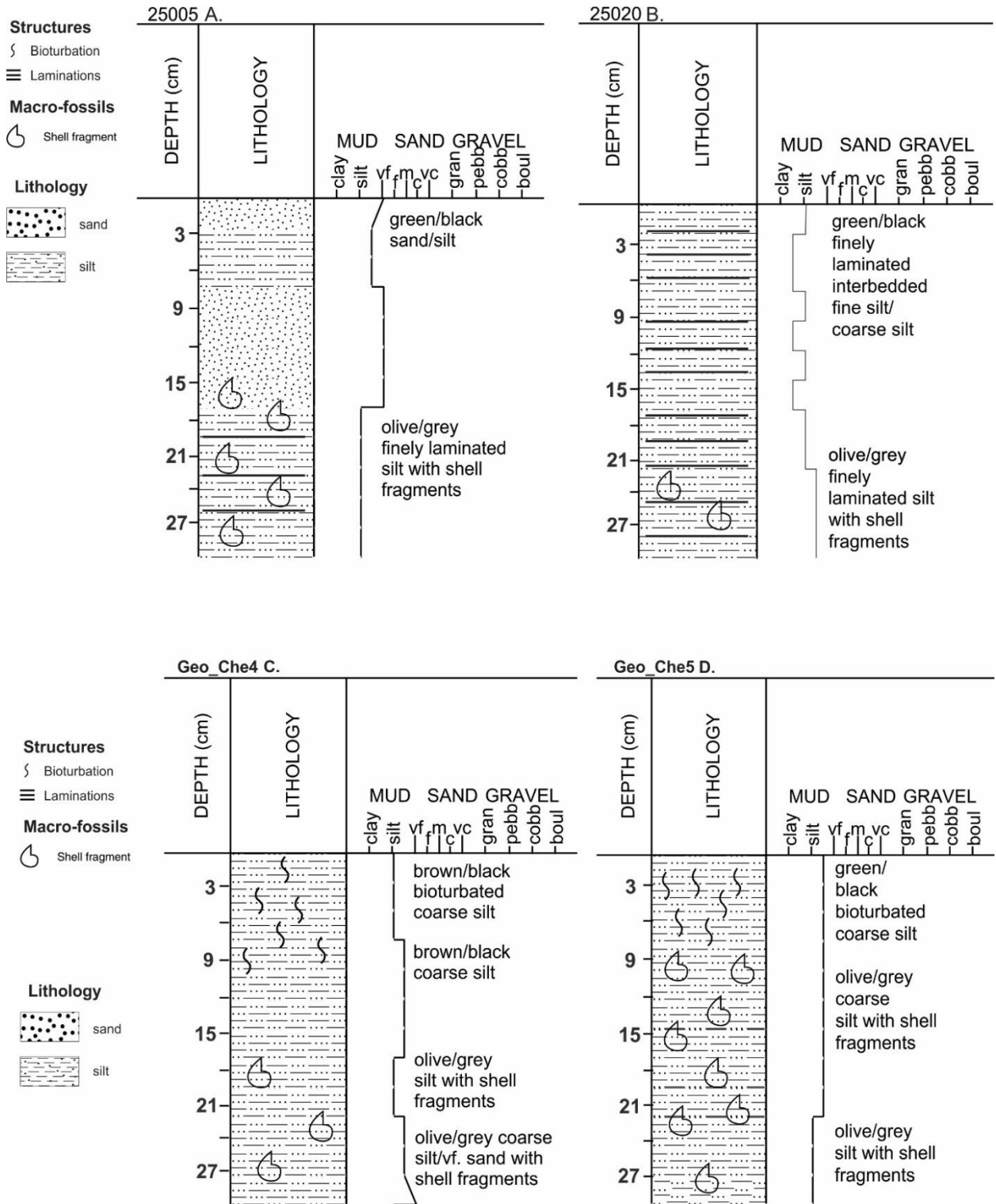


**Figure S1:** Lithology columns with grain size distribution for cores 25005, 25020, Geo\_Che4, and Geo\_Che5.

**Table S4:** Particle size analysis data for cores 25005, 25020, Geo\_Che4, and Geo\_Che5

Core	Interval (cm)	Mid-point	% Sand	% Clay	% Silt	Moment Mean Grain Size	Moment Std. Dev. for Mean Grain Size	Moment Skewness
<b>25005</b>	0-1	0.5	78.2	2.5	19.3	3.6	1.1	2.7
	1-2	1.5	55.5	5.6	38.9	4.2	1.5	1.6
	2-4	3.0	64.2	4.2	31.6	3.8	1.3	2.1
	4-6	5.0	70.3	3.6	26.2	3.7	1.3	2.3
	6-8	7.0	72.6	4.0	23.4	3.7	1.3	2.4
	8-10	9.0	76.1	3.3	20.7	3.6	1.3	2.4
	12-14	13.0	14.3	7.7	78.1	5.2	1.4	1.0
	16-18	17.0	7.2	9.2	83.6	5.5	1.4	1.3
	20-22	21.0	8.1	8.8	83.1	5.5	1.4	1.2
	24-26	25.0	5.1	7.3	87.6	5.5	1.3	1.3
<b>25020</b>	1-2	1.5	3.2	17.6	79.2	6.2	1.4	0.9
	2-4	3.0	1.7	18.4	79.9	6.3	1.4	0.9
	4-6	5.0	2.0	18.4	79.6	6.2	1.4	0.9
	6-8	7.0	2.3	17.8	79.9	6.2	1.4	0.9
	8-10	9.0	1.4	19.7	79.0	6.3	1.4	1.0
	12-14	13.0	5.0	19.6	75.5	6.1	1.6	0.7
	16-18	17.0	2.5	24.0	73.5	6.4	1.6	0.7
	20-22	21.0	14.7	16.1	76.6	5.6	1.7	0.8
	24-26	25.0	23.6	18.0	58.4	5.5	1.9	0.7
	<b>Geo_Che4</b>	0-1	0.5	29.5	11.3	59.2	4.9	1.7
1-2		1.5	31.8	9.4	58.8	4.9	1.6	1.1
2-4		3.0	39.8	7.1	53.1	4.6	1.5	1.3
4-6		5.0	37.3	5.8	56.9	4.6	1.5	1.2
6-8		7.0	38.5	6.5	55.0	4.6	1.6	1.3
8-10		9.0	35.8	9.3	54.9	4.8	1.6	1.2
12-14		13.0	28.3	6.6	65.1	4.9	1.5	1.1
18-20		19.0	37.5	5.8	56.7	4.6	1.5	1.3
22-24		23.0	40.3	5.8	53.9	4.5	1.5	1.3
<b>Geo_Che5</b>		0-1	0.5	3.1	14.2	82.8	6.0	1.4
	1-2	1.5	3.5	11.4	85.1	5.8	1.4	1.0
	2-4	3.0	2.3	15.9	81.8	6.1	1.5	0.9
	4-6	5.0	2.6	15.1	82.3	6.0	1.5	0.9
	6-8	7.0	3.3	12.1	84.6	5.9	1.4	1.0
	8-10	9.0	3.1	13.4	83.5	5.9	1.4	1.0
	12-14	13.0	7.0	8.5	84.6	5.6	1.3	0.9
	18-20	19.0	2.0	17.3	80.7	6.1	1.5	0.9
	22-24	23.0	6.1	9.4	84.5	5.7	1.3	1.0

VITA

Jessica Cofrancesco

Candidate for the Degree of

Master of Science

Thesis: GEOCHEMICAL SIGNATURES FOR REDEPOSITIONAL ENVIRONMENTS BENEATH OXYGEN MINIMUM ZONES: THE BENGUELA UPWELLING SYSTEM OFFSHORE NAMIBIA

Major Field: Geology

Biographical:

Education:

Completed the requirements for the Master of Science in Geology at Oklahoma State University, Stillwater, Oklahoma in December, 2016.

Completed the requirements for the Bachelor of Science in Geology at California State University Los Angeles, Los Angeles, CA/USA in 2014.

Professional Memberships:

Phi Theta Kappa, American Association of Petroleum Geologists (AAPG), Tulsa Geological Society (TGS), West Coast Geological Society (WCGS), Regional Graduate Network in Oceanography (RGNO), California State University of Los Angeles (CSULA) Alumni Association